UNIVERSITAT POLITÈCNICA DE CATALUNYA
BARCELONATECH
Escola d'Enginyeria de Barcelona Est

MASTER THESIS

Master's Degree in Interdisciplinary and Innovative Engineering

RECONFIGURABLE PHOTOVOLTAIC SYSTEMS. PRACTICAL APPROACH TO TEAM SYSTEMS

Report and Annex

Author: Roohollah Afzali
Supervisor: Guillermo Velasco Quesada
Department Electronic Engineering

Call: 2023, July

Abstract

Although solar energy plays a vital role in pursuing sustainable development and addressing climate change, several challenges hinder its widespread development. Solar power generation relies on sunlight availability, making it intermittent and dependent on weather conditions. Additionally, the initial cost, integration into power grids, and storage of surplus energy present serious challenges. However, ongoing research and development efforts aim to overcome these obstacles and enhance the efficiency, affordability, and reliability of solar energy systems.

Accordingly, the objective of this thesis is to explore the efficiency of grid-connected photovoltaic (GCPV) systems. The significance lies in the fact that even a slight improvement in efficiency can have a profound impact, making solar energy more accessible and cost-effective.

In this regard, a numerical method is used to evaluate the energy flows in the system and the plant-oriented (PO) configuration is selected as the architecture of GCPV systems. Arduino, relay, solar array simulator, power meter, ports, inverters, and MATLAB form a GCPV system.

Fixed and team systems which are arrangements of inverters and PV arrays are selected to be emulated. Fixed systems are working with two parallel inverters and team systems are able to select working with one or two inverters. In this case, some calculations are done to find the best switching points. Additionally, a switching problem arises which has been addressed in the report.

The emulation of total energy capturing and processing processes have been conducted and the results are compared. It is worth mentioning that these emulations are performed according to several weather conditions or irradiation levels.

Finally, the results of these real-time emulations show the disparity in the energies delivered to the grid that proves the effect of the configuration on efficiency.

Resum

Encara que l'energia solar juga un paper vital en la recerca de desenvolupament sostenible i en l'abordatge del canvi climàtic, diversos reptes dificulten el seu desenvolupament generalitzat. La generació d'energia solar depèn de la disponibilitat de llum solar, la qual cosa la fa intermitent i dependent de les condicions climàtiques. A més, el cost inicial, la integració en les xarxes elèctriques i l'emmagatzematge de l'excedent d'energia presenten reptes importants. No obstant això, els esforços continus de recerca i desenvolupament tenen com a objectiu superar aquests obstacles i millorar l'eficiència, l'accessibilitat i la fiabilitat dels sistemes d'energia solar.

En conseqüència, l'objectiu d'aquesta tesi és explorar l'eficiència dels sistemes fotovoltaics connectats a la xarxa (GCPV, per les seves sigles en anglès). La importància rau en el fet que fins i tot una lleugera millora en l'eficiència pot tenir un gran impacte, fent que l'energia solar sigui més accessible i rendible.

En aquest sentit, s'utilitza un mètode numèric per avaluar els fluxos d'energia en aquests sistemes i es selecciona la configuració orientada a la planta (PO) com l'arquitectura dels sistemes GCPV. Controladors Arduino, commutadors controlats, simuladors de generadors fotovoltaics, mesuradors d'energia i inversors fotovoltaics de connexió a la xarxa formaran part dels sistemes GCPV a provar, utilitzant MATLAB com a programari de control.

Es simularan sistemes fotovoltaics de configuració estàtica i sistemes fotovoltaics de configuració dinàmica del tipus TEAM. Els sistemes de configuració estàtica funcionen amb dos inversors en paral·lel i els sistemes TEAM poden seleccionar treballar amb un o dos inversors. En aquest cas, es realitzen alguns càlculs per trobar els millors punts de commutació. A més, sorgeix un problema de commutació que s'aborda en l'informe.

S'han dut a terme les simulacions dels processos totals de captura i processament d'energia i s'han comparat els resultats. Val la pena destacar que aquestes simulacions es realitzen segons diferents condicions climàtiques o nivells de radiació.

Finalment, els resultats d'aquestes simulacions en temps real mostren la disparitat en les energies lliurades a la xarxa, la qual cosa demostra l'efecte de la reconfiguració en l'eficiència.

Resumen

Aunque la energía solar desempeña un papel vital en la búsqueda del desarrollo sostenible y en abordar el cambio climático, varios desafíos dificultan su desarrollo generalizado. La generación de energía solar depende de la disponibilidad de luz solar, lo que la hace intermitente y dependiente de las condiciones climáticas. Además, el costo inicial, la integración en las redes eléctricas y el almacenamiento del excedente de energía presentan desafíos importantes. Sin embargo, los esfuerzos continuos de investigación y desarrollo tienen como objetivo superar estos obstáculos y mejorar la eficiencia, la accesibilidad y la confiabilidad de los sistemas de energía solar.

En consecuencia, el objetivo de esta tesis es explorar la eficiencia de los sistemas fotovoltaicos conectados a la red (GCPV, por sus siglas en inglés). La importancia radica en el hecho de que incluso una ligera mejora en la eficiencia puede tener un gran impacto, haciendo que la energía solar sea más accesible y rentable.

En este sentido, se utiliza un método numérico para evaluar los flujos de energía en estos sistemas y se selecciona la configuración orientada a la planta (PO) como la arquitectura de los sistemas GCPV. Controladores Arduino, conmutadores controlados, simuladores de generadores fotovoltaicos, medidores de energía, inversores fotovoltaicos de conexión a red formarán parte de los sistemas GCPV a ensayar, utilizándose MATLAB como software de control.

Se emularán sistemas fotovoltaicos de configuración estática y sistemas fotovoltaicos de configuración dinámica del tipo TEAM. Los sistemas de configuración estática funcionan con dos inversores en paralelo y los sistemas TEAM pueden seleccionar trabajar con uno o dos inversores. En este caso, se realizan algunos cálculos para encontrar los mejores puntos de conmutación. Además, surge un problema de conmutación que se aborda en el informe.

Se han llevado a cabo las emulaciones de los procesos totales de captura y procesamiento de energía, y se han comparado los resultados. Vale la pena mencionar que estas emulaciones se realizan de acuerdo a varias condiciones climáticas o niveles de radiación.

Finalmente, los resultados de estas emulaciones en tiempo real muestran la disparidad en las energías entregadas a la red, lo que demuestra el efecto de la reconfiguración en la eficiencia.

Appreciations

I am incredibly grateful for the unwavering support and guidance of my supervisor, Guillermo, whose contribution was indispensable in bringing this project to fruition. I want to express my deepest appreciation for his patience, dedication, and constructive feedback, which played a pivotal role in shaping the final outcome of my work.

I want to express a heartfelt acknowledgment to my parents for their continuous support and understanding throughout my life. Your prayers for me have been a source of strength and encouragement, sustaining me through every step of my journey.

Additionally, I am deeply grateful to my supportive brother, Hamed, for being both a dear friend and companion to me. To my dear sister, Razieh, thank you for your kind encouragement.

Special thanks to my lovely aunt, Ehteram, and my dear cousin, Meisam, for their constant support and assistance. Your presence and unwavering support have meant the world to me.

Finally, I would like to thank God, for letting me through all the difficulties.

Glossary:

PV: photovoltaic

PO: Plant Oriented

T: Temperature

MPP: Maximum Power Point

STC: Standard Test Conditions

SPV: solar photovoltaic System

SAS: Solar Array Simulator

AC: Alternating Current

DC: Direct Current

G: Irradiance

GCPV: Grid Connected Photovoltaic

$R_{S\ OPT}$: Optimal value of the sizing ratio

PVG: PV Generator

$W_{P:}$ Watt peak

GPIB: General Purpose Interface Bus

.

Index

1. Introduction

The crisis triggered by Russia's invasion of Ukraine has accelerated renewable energy deployment in the European Union, driving the bloc to urgently reduce its dependence on Russian natural gas imports [1]. This means that renewable energy should not be considered simply as an economic or environmental issue but as a powerful new policy maker.

As part of the REPowerEU plan, this strategy aims to bring online over 320 GW of solar photovoltaic by 2025 (more than doubling compared to 2020) and almost 600 GW by 2030. The EU's renewable energy policies helped bring PV costs down by 82% over the last decade, turning it into one of the most competitive sources of electricity in the EU. Solar energy, combined with energy efficiency, protects European citizens from the volatility of fossil fuel prices [2].

In the long run, renewables and energy efficiency will play the dominant role in accelerating the global energy transition process, which is pivotal to achieving the 1.5°C climate target under the Paris Agreement [3].

These facts indicate that by simultaneously enhancing the capacity and efficiency of solar energy, it can assume a substantial role in the global energy market. Hence in this thesis, different possible photovoltaic systems are compared to achieve higher efficiency.

1.1. Objective

Generally, PV cells can be connected to the grid by inverters. Inverters provide alternating current that is synchronized with the grid. The inverter rated power would be chosen in order to maximize the energy delivered to the grid. Several configurations of inverters and PV arrays are proposed to connect PV cells to the grid. These systems can be divided into fixed and reconfigurable systems. Theoretically, some of them have higher energy efficiency, and this study aims to investigate these claims.

Specifically, the aim of this thesis is to perform calculations to design a reconfigurable system that can be compared with a fixed system. The ultimate goal is to find a way to increase the energy efficiency of Photovoltaic Generators (PVGs).

1.2. Scope

Practically, MIX and team systems are two main types of reconfigurable systems, and this project focuses on team systems and fixed systems. It is worth mentioning that a solar array simulator is utilized to mimic the behavior of PV cells, and emulations are performed according to daily data sets.

To evaluate the systems, three distinct weather conditions, namely sunny, cloudy, and partly sunny days, are defined. The systems are tested across multiple irradiance levels, and comparative analyses are performed to identify the optimal configuration for each specific condition.

2. Grid-Connected PV Systems

The plant-oriented (PO) configuration, depicted in figure 2.1, is the most predominant architecture of GCPV systems due to its simplicity and low cost per kW_P. This configuration is based on a single set of series-parallel electrically interconnected PV modules. This arrangement, generally known as a PV generator (PVG), can be considered the energy-caption subsystem. In addition, the PVG is linked to the grid through a single central inverter, which is considered the energy-processing subsystem. Obviously, this inverter is used to extract the maximum power from the PVG and transfer it properly to the grid. [4]

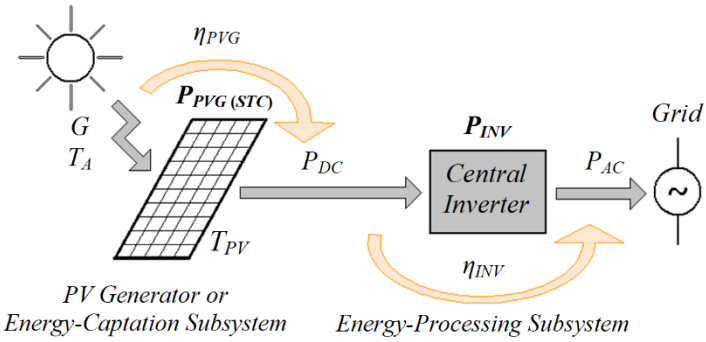

Figure 2.1. Elements in a GCPV system based on PO configuration.

2.1. Sizing Ratio

In this analysis, the focus is specifically on the PV-to-Inverter sizing ratio [5], chosen from numerous available terms that describe this concept. equation (2.1) represents this ratio mathematically, where the numerator represents the peak power of the PVG, (given in W_p), and the denominator represents the rated power of the central inverter measured at the AC side.

$$R_s = \frac{P_{PVG\,(STC)}}{P_{INV}} \qquad \textbf{(Eq. 2.1)}$$

As is shown in equation (2.2), the optimal value of the sizing ratio will lead to the maximum level of energy efficiency during a period. It should be noted, E_{AC} denotes the energy supplied to the power grid by the central inverter, while E_{DC}represents the available energy at the inverter's input. P_{AC} and P_{DC} indicate the respective magnitudes of power involved.

$$\eta_E(R_{S\,OPT}) = max\left(\frac{E_{AC}}{E_{DC}}\right) = max\left(\frac{\int_0^T P_{AC}(t)\,dt}{\int_0^T P_{DC}(t)\,dt}\right) \quad \textbf{(Eq. 2.2)}$$

This equation provides insight into how the optimal sizing ratio ($R_{S\,OPT}$) varies depending on the site and time. Irradiance G and ambient temperature T_A which define DC and AC powers, vary based on both the location and time. Therefore, the optimal sizing ratio shows the same behavior. Moreover, it relies on the specific time interval T considered for its computation (hour, day, month, year…).

2.2. Photovoltaic generator model

This study is performed based on the model for a generic PVG that is presented in [6]. The purpose of these numerical models is the evaluation of the energy flows in the system and, thus, the evaluation of the system's energy efficiency. The mathematical models and the principle for the description of GCPV system elements can be formulated by equation (2.3), where:

- $P_{DC}(t)$ is the PVG output power (given in W).
- η_{PVG} represents the PVG efficiency related to the material used in PV cell construction.
- $G(t)$ indicates the irradiance incident on the PVG plane (W/m^2).
- β represents the thermal power coefficient of the PVG material (1/ºC).
- $T_{PVG}(t)$ is the PVG operating temperature (ºC).
- T_R represents the reference temperature (25 ºC).
- S_{PVG} is the PVG surface (m^2).

$$P_{DC}(t) = \eta_{PVG} \cdot G(t) \cdot [1 - \beta \cdot (T_{PVG}(t) - T_R)] \cdot S_{PVG} \quad \textbf{(Eq. 2.3)}$$

Equation (2.4), proposed in [7], presents an expression to estimate the value of the PVG operating temperature ($T_{PVG}(t)$), where:

- $T_A(t)$ is the ambient temperature (ºC).
- $G(t)$ shows the irradiance incident on the PVG plane (W/m^2).
- **k** represents the PVG thermal coefficient called the coefficient of Ross (ºC ·m^2/W).

$$T_{PVG}(t) = T_A + k \cdot G(t) \quad \textbf{(Eq. 2.4)}$$

As suggested by [8], the Ross coefficient (k) is assigned typical values of 0.025 for PVG installations on a flat surface (flat roof) with good ventilation, and 0.050 for PVG integrated into buildings (commonly on façades or sloped roofs) where ventilation is generally poorer.

2.3. Simulation procedure for sizing ratio estimation

In reference [9], a simulation procedure is presented for calculating the optimal sizing ratio value in terms of yearly energy production. Figure 2.2 illustrates the simplified block diagram of this procedure.

The ratio between the energy injected into the grid (E_{AC}) and the energy delivered by the PVG (E_{DC}) defines the energy efficiency of the GCPV system (η_E). The irradiance $G(t)$ and ambient temperature $T_A(t)$ data at the considered location and using a PVG numerical model enable us to compute the available power at the inverter input ($P_{DC}(t)$) and E_{DC} as well. Considering the inverter efficiency model, the inverter output power ($P_{AC}(t)$) and E_{AC} can also be estimated.

Formally speaking, this simulation procedure only estimates the energy efficiency of the GCPV system (η_E) for a given value of R_S, since the values of P_{INV} and $P_{PVG(STC)}$ remain constant throughout the simulation.

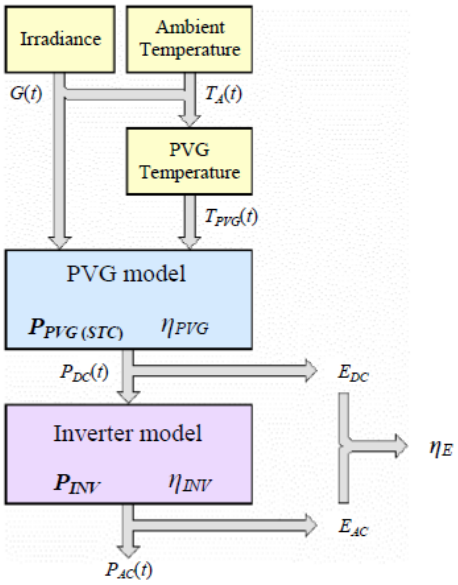

Figure 2.2. Block diagram of the simulation procedure utilized to obtain the $R_{S\,OPT}$ value.

Therefore, the determination of $R_{S\,OPT}$ requires multiple and iterative executions of this procedure introducing a slight modification of R_S between simulations. Once all simulations have been completed, the value of $R_{S\,OPT}$ will be the one corresponding to the highest energy efficiency (η_E) computed.

2.4. Adaptive Sizing Ratio Systems

As mentioned in section 2.1, the sizing ratio value of the GCPV system is determined by both the nominal power of the PVG and the rated power of the central inverter. Moreover, the optimal sizing ratio is a time-dependent variable. Hence, the utilization of a PV system at the optimal sizing ratio point has been considered. The optimal sizing of a GCPV system based on a PO configuration (figure 2.1) involves determining the optimal relationship between the nominal or peak power of the energy capture subsystem (P_{PVG}) and the nominal power of the energy processing subsystem (P_{INV}) that is used.

In practical applications, there are typically two types of reconfigurable systems:

- MIX systems, which can modify the value of the central inverter rated power connected to a PVG.
- Team systems, which can modify the nominal power of the PVG connected to a central inverter.

2.4.1. MIX Systems

In 2003, the company Fronius introduced the term MIX (Master Inverter X-change). It is used to define the reconfigurable operation principle of some series of their grid-connected PV inverters [10]. The companies Emerson Electric [11], ABB [12], and Vacon [13] use the term Multimaster to describe a very similar reconfigurable operation principle applied to central inverters.

The system consists of a single PVG serving as the energy-capturing subsystem and one energy-processing subsystem. The energy processing subsystem comprises multiple inverters connected in parallel, with one designated as the leader and the rest acting as follower devices. In this regard, the number of inverters connected in parallel to the PVG will depend on the energy generated by the PVG at any moment.

Figure 2.3 represents an example of a GCPV system based on the MIX or Multimaster concept. This system consists of three inverters (m = 3) capable of operating in parallel connection.

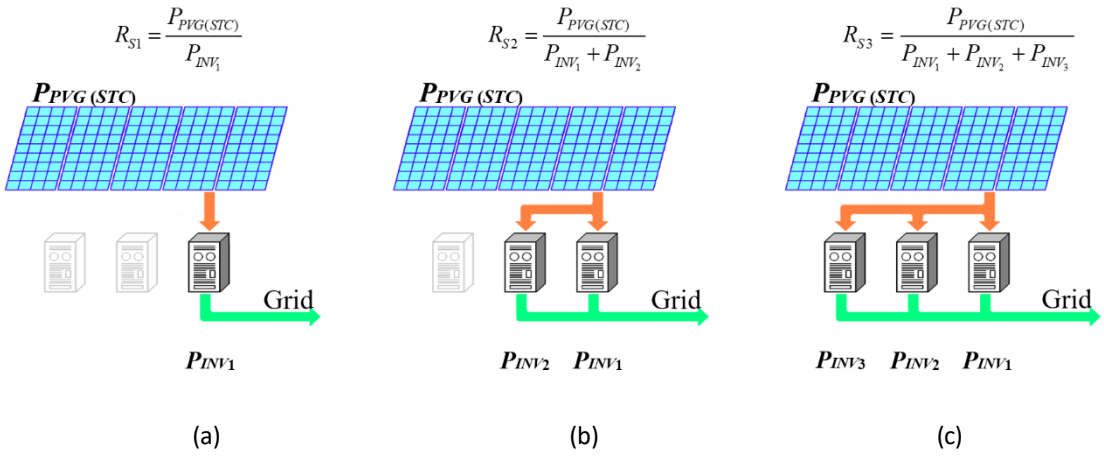

Figure 2.3. MIX system based on three inverters to set the energy-processing subsystem.

The depicted configuration in figure 2.3(a) represents the setup utilized during periods of low energy production, and it has the higher R_S value. Once the energy production of the PVG surpasses a specific threshold, it is necessary to transition to the configuration presented in figure 2.3(b). This configuration exhibits a lower RS value compared to the previous scenario. Lastly, figure 2.3(c) corresponds to the periods of greatest energy production. It has the lower R_S value of the three possible configurations.

2.4.2. Team Systems

The term team was introduced in 2002 by the company SMA Solar Technology AG to designate the reconfiguration strategy adopted in some series of grid-connected PV inverters. Since then, the application of this concept to the line of central inverters can be found in several company publications [14 - 15].

This method concentrates on modifying the value of the nominal power of the PVG connected to a single inverter, whose maximum power is constant. Team systems are composed of an equal initial number of PV arrays (n) and inverters. The grouping or division of the PV generators connects one or more of the available inverters to increase (or decrease) the nominal power of the resulting PV generators. These actions are done based on the available output power of PV arrays and the rated power of the used inverters.

In order to simplify the analysis of this kind of system, two hypotheses concerning the team architecture are assumed:

1) The n PV arrays have the same nominal power (it is noted as P_{PVG})

2) The n used inverters have the same rated power; that is, $P_{INV1} = P_{INV2} = \ldots = P_{INVn} = P_{INV}$.

Figure 2.4 shows the various configurations of a team based GCPV system, which comprises four PV arrays and four inverters (n = 4).

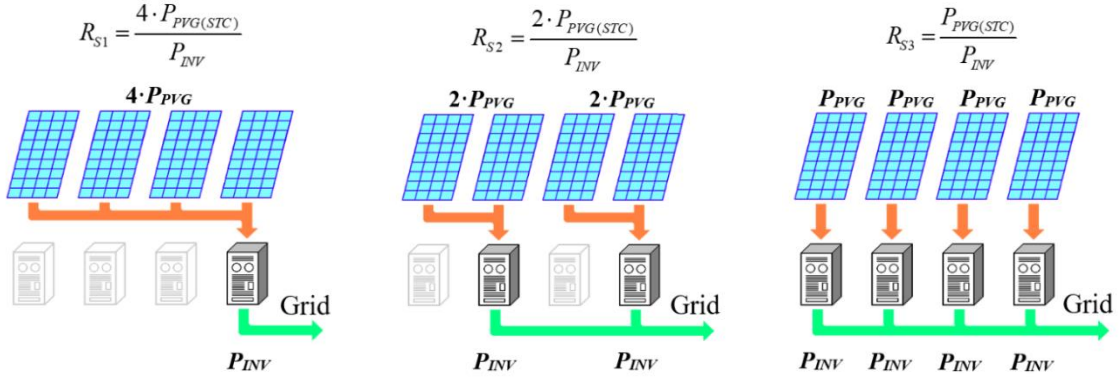

(a) (b) (c)

Figure 2.4. Three available configurations and the corresponding RS value for a team GCPV system with n = 4.

The configuration shown in figure 2.4(a) is used in periods of low insolation (lower energy production). In this case, the union of the four available basic PV arrays, connected to a single inverter provides the highest value of R_S.

The second case is related to the higher energy production of the PVG and exceeding a certain threshold, where the system configuration is changed to the format shown in figure 2.4 (b). It is evident that the PV generator is divided into two equal parts and each new PVG is connected to one inverter. Therefore, this new configuration has two equal sizing ratio factors, but half the value obtained in the previous configuration.

The last format corresponds to the configuration to be used during the periods of highest insolation. As figure 2.4 (c) shows, the system consists of four PV generators, and each PVG is connected to a single inverter performing four subsystems with equal R_S factors (the smaller value when compared with the two previous configurations).

3. Team System characterization

3.1.1. Central inverter model

The available power at the inverter output ($P_{AC}(t)$) depends on both the inverter input power (P_{DC}) and the inverter's efficiency (η_{INV}). Among several models representing the inverter's efficiency curve, the model presented in [16] is commonly used. This model is only applicable for input power ranges lower than the inverter rated power (P_{INV}) and it is given by equation (3.1).

$$\boldsymbol{\eta_{INV} = \frac{p_{dc}(t)}{k_0 + k_1 \cdot p_{dc}(t) + k_2 \cdot p_{dc}^2(t)} \quad being \quad p_{dc}(t) = \frac{P_{DC}(t)}{P_{INV}}} \qquad \textbf{(Eq. 3.1)}$$

Where:

- $\boldsymbol{p_{dc}(t)}$ is the inverter input power normalized to the inverter rated power.
- $\boldsymbol{k_0}$ stands for the losses coefficient at no load.
- $\boldsymbol{k_1}$ and $\boldsymbol{k_2}$ stand for coefficients corresponding to losses varying linearly and quadratically with the inverter current.

For input power ranges higher than the inverter nominal power, the models commonly utilized assume the limitation of the inverter output power to this nominal value, as is shown in equation (3.2).

$$\boldsymbol{P_{DC}(t) = P_{INV} \quad \rightarrow \quad p_{dc}(t) = \frac{P_{DC}(t)}{P_{INV}} = 1} \qquad \textbf{(Eq. 3.2)}$$

3.1.2. K Coefficients

In order to obtain K parameters in equation (3.1), a specified emulation has been conducted. A range of irradiance [0 - 1000 W/m^2] is applied as input and after measurements and calculations the efficiency curve is plotted. The last step of this process is fitting curve to find the best values of k_0, k_1 and k_2. The following figures show the effect of irradiance changes on AC power (figure 3.1), DC power (figure 3.2), and figure 3.3 depicts the efficiency curve.

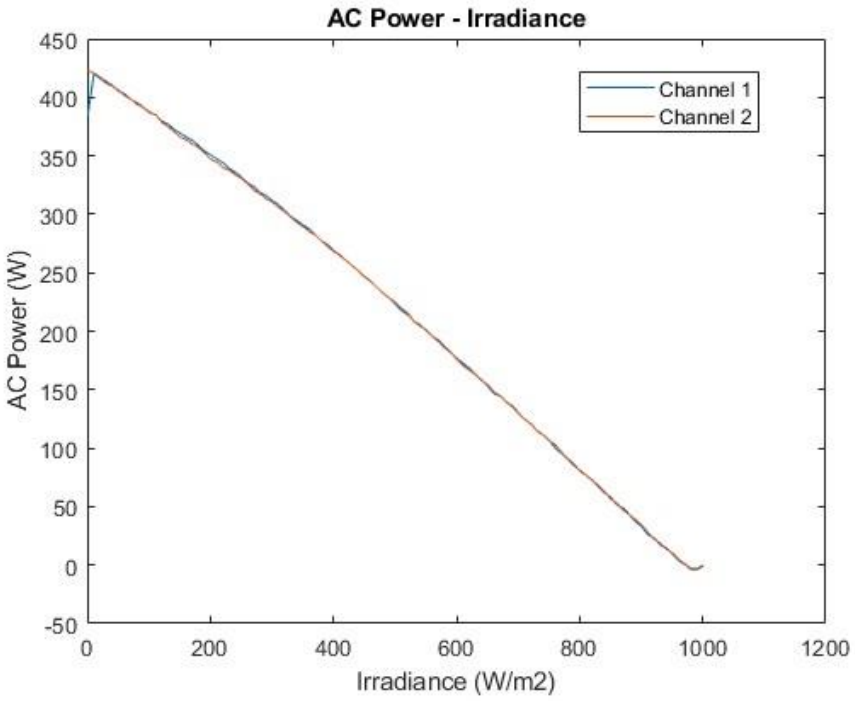

Figure 3.1. Delivered AC power vs. irradiance.

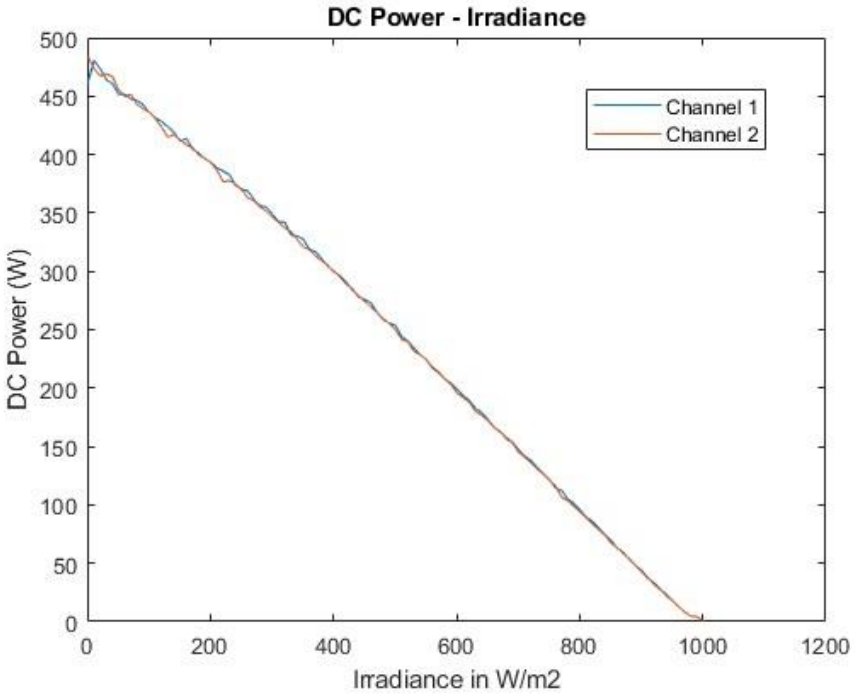

Figure 3.2. Generated DC power vs. irradiance.

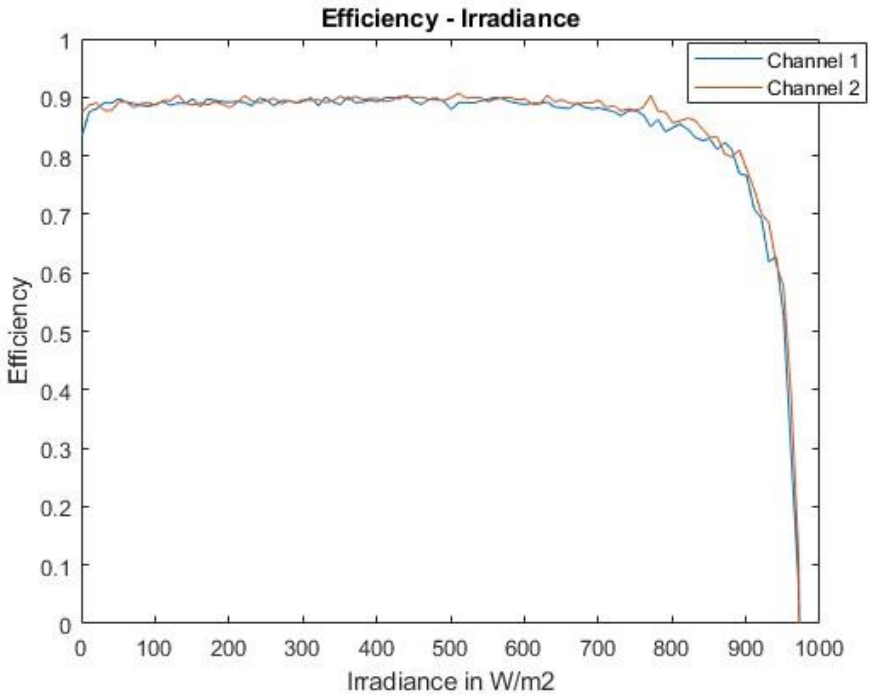

Figure 3.3. Efficiency vs. irradiance.

With the intention of comparison, K coefficients are computed from four datasets. Two sets of them are obtained independently from each SAS channel. The third case is the merged data of channels while the fourth set is the cleaned data, which is acquired by removing outliers from the merged dataset.

It should be noted that the fitting curve process is conducted on an efficiency curve based on normalized DC power. The following figures (3.4, 3.5, 3.6, and 3.7) show fitting curves in all situations.

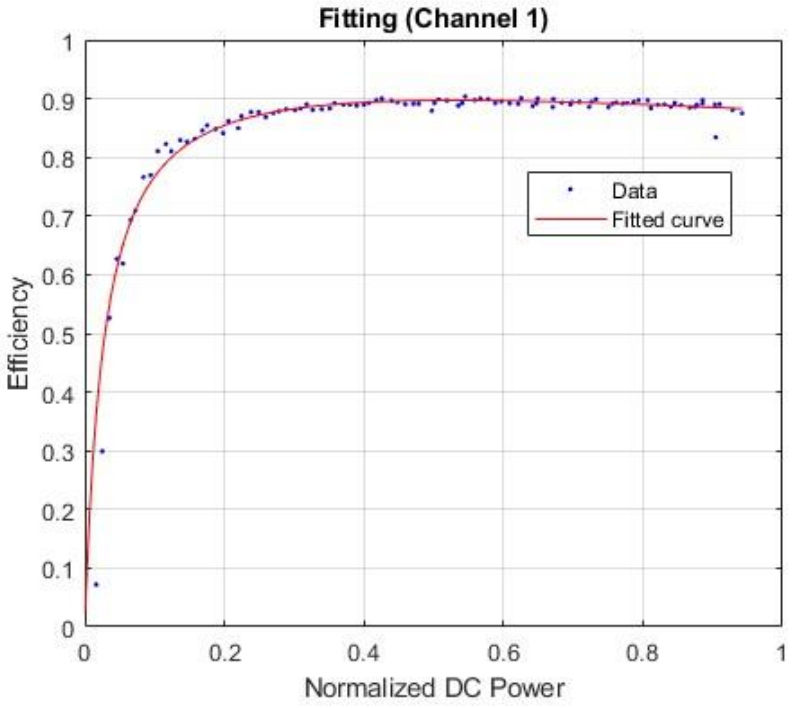

Figure 3.4. The fitting curve for the first channel data set.

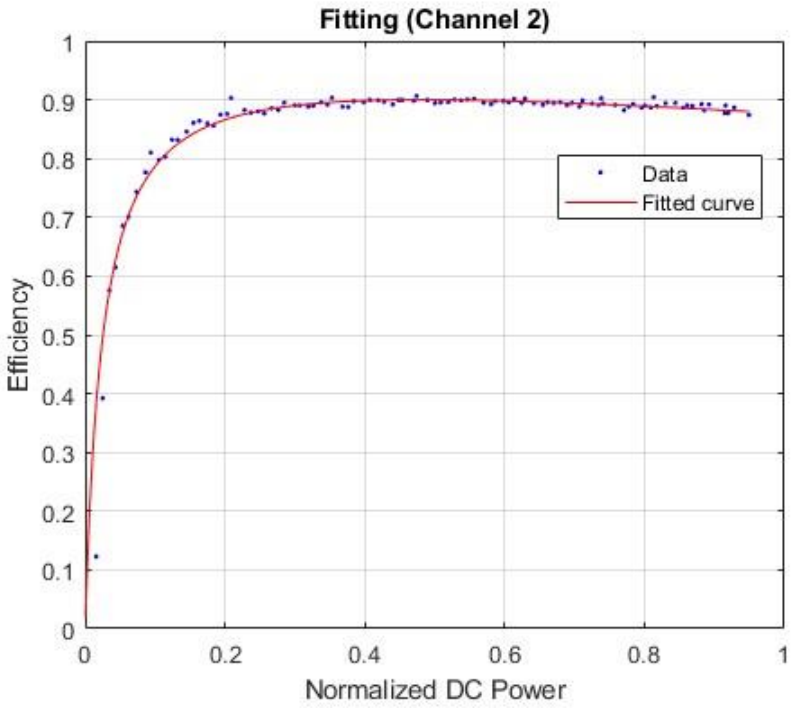

Figure 3.5. The fitting curve for the second channel data set.

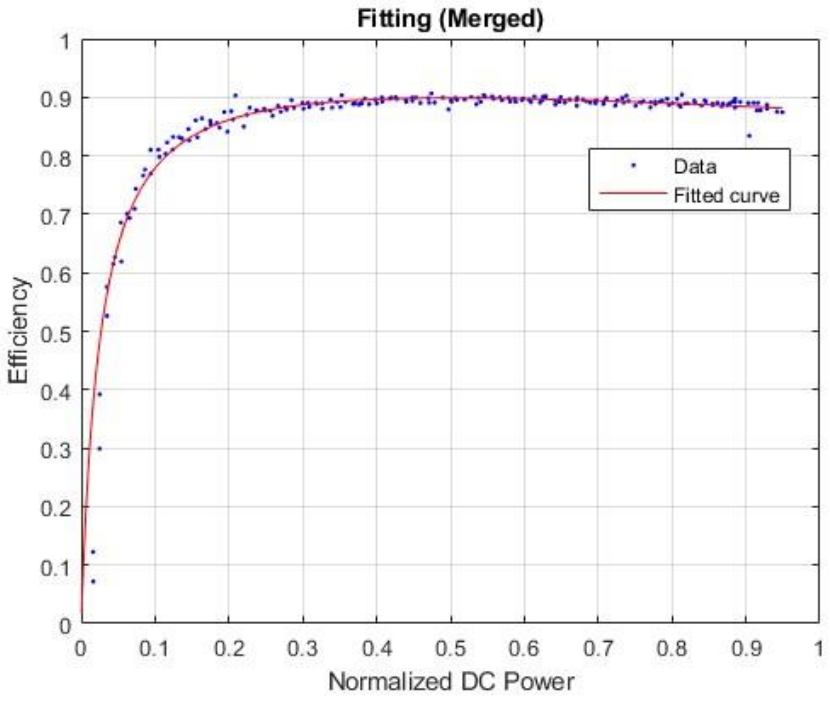

Figure 3.6. The fitting curve for the merged data set.

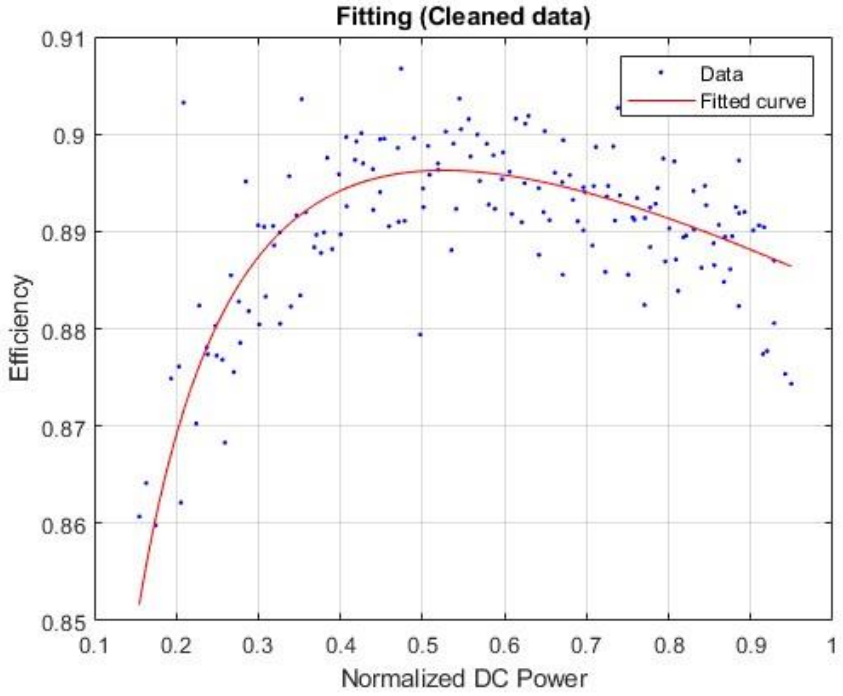

Figure 3.7. The fitting curve for cleaned data set.

	k0	*k1*	*k2*
Channel 1	*0.027444*	*0.096693*	*1.004568*
Channel 2	*0.026962*	*0.110187*	*0.999356*
Merged data	*0.027626*	*0.105882*	*1.000143*
Cleaned data	*0.021879*	*0.073051*	*1.031472*

Table 3.1. K coefficients comparison according to four data sets.

Table 3.1 shows the calculated values of K coefficients. The results are nearly identical and the calculations and in the subsequent section, the calculations will only utilize the coefficients obtained from the merged and cleaned data.

3.1.3. Threshold

In this step the analytical expressions are considered to determine the power thresholds required for grouping or dividing. In the specific case of the team system, which comprises two inverters, the focus is on determining when to transition between using one inverter and utilizing both inverters and vice versa.

In this way, the value of the threshold power to pass from the power processor formed by $a–1$ inverters in parallel to the formed by a inverters in parallel (denoted as P_{Ua}) will be calculated from the intersection of the curves of efficiency of the two power processors involved, as shown equation (3.3).

$$\boldsymbol{\eta_{INV\,a-1}(P_{Ua}) = \eta_{INV\,a}(P_{Ua}) \qquad being\ \ a > 1} \qquad \textbf{(Eq. 3.3)}$$

Applying in equation (3.1) this condition, equation (3.4) is obtained:

$$\frac{\frac{P_{Ua}}{(a-1)\cdot P_{INV}}}{k_0+k_1\cdot\frac{P_{Ua}}{(a-1)\cdot P_{INV}}+k_2\cdot\frac{{P_{Ua}}^2}{(a-1)^2\cdot {P_{INV}}^2}} = \frac{\frac{P_{Ua}}{a\cdot P_{INV}}}{k_0+k_1\cdot\frac{P_{Ua}}{a\cdot P_{INV}}+k_2\cdot\frac{{P_{Ua}}^2}{a^2\cdot {P_{INV}}^2}} \qquad \textbf{(Eq. 3.4)}$$

This expression shows the value of the power threshold for the reconfiguration of the energy-processing subsystem in both cases: Addition or subtraction of one inverter in the parallel interconnection.

$$\boldsymbol{P_{UD} = P_{INV}\cdot\sqrt{\frac{2\cdot K_0}{K_2}}\ ,\ P_{UG} = P_{INV}\cdot\sqrt{\frac{K_0}{2\cdot K_2}}} \qquad \textbf{(Eq. 3.5)}$$

Where:

- $\boldsymbol{P_{INV}}$ stands for the rated power of the used inverters.

- k_0 and k_2 are the parameters of the used inverters efficiency curve given in equation (3.1).

These thresholds are obtained from the solution of equation (3.4) and are shown in equation (3.5). As shown in figure 3.8, when the output power of two PV generators reaches the value P_{UG}, they must be grouped, and it must be divided into two PV generators when the output power of one PV generator reaches the value P_{UD}.

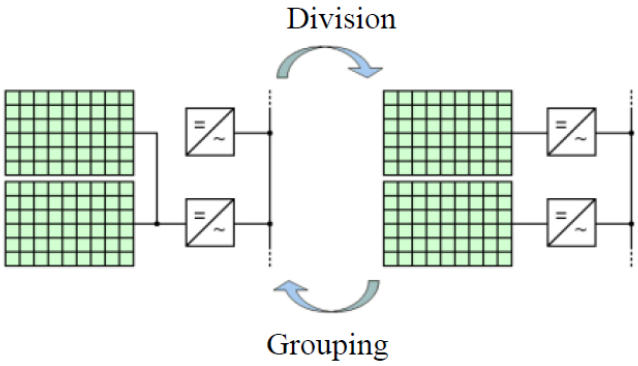

Figure 3.8. Reconfiguration actions of PV generators in team-based systems.

Using an adaptation of the simulation procedure described in figure 2.2 and the reconfiguration thresholds shown in equation (3.5), figure 3.9 shows the value of the yearly energy efficiency (η_E) in terms of the number of basic PV generators (n) available in the considered team based GCPV system. The values of n considered are n = 1, 2, 4, and 8 (powers of two), being the case n = 1 corresponding to a nonreconfigurable GCPV system.

The results show the increase in the annual energy efficiency of the GCPV system by increasing the number of basic PV generators (n). However, the tendency to saturation in this relationship is also observed.

The greatest increase in energy efficiency, 0.71%, occurs when going GCPV system with static configuration (n = 1) to the use of two PV generators (n = 2). The use of four PV generators (n = 4) instead of two only means an increase of 0.27% in the annual energy efficiency. This means that more complex and expensive systems do not significantly increase efficiency.

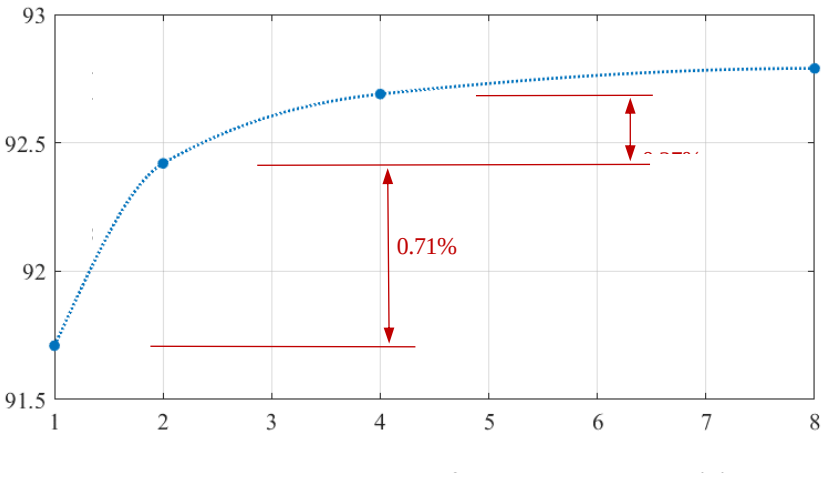

Figure 3.9. Relationship between annual energy efficiency (η_E) and the number of basic PV generators (n) used in a team-based GCPV system of up to n = 8.

The implemented experimental setup used for the characterization of GCPV systems based on the team concept is shown in figure 3.10. A system that uses only two photovoltaic generators (n = 2) is implemented, because this configuration is the one that supposes a greater increase in the annual energy efficiency (0.71% of increase).

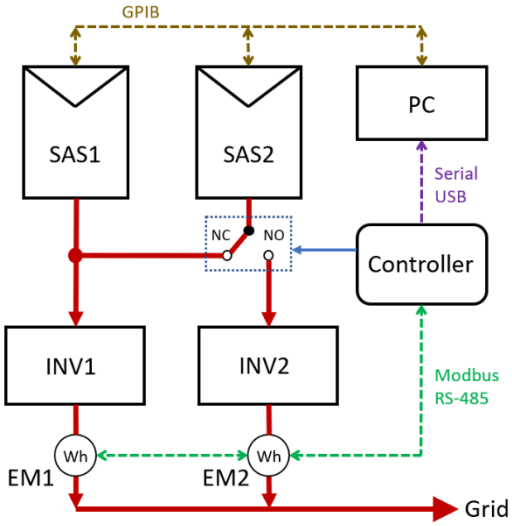

Figure 3.10. Diagram of the experimental set used for a team-based GCPV system characterization.

Finally, table 3.2 represents the calculated thresholds that are obtained from the solution of equation (3.5). Although the emulations are performed based on the results obtained from using cleaned data, Section 5.5 specifically examines the effects of employing different thresholds.

	P_{UG}	P_{UD}
Merged data	*58.93201*	*117.864019*
Cleaned data	*51.469652*	*102.939305*

Table 3.2. Thresholds obtained from two data sets.

4. Emulations

4.1. Hardware and Software

4.1.1. Solar Array Simulator (SAS)

The Solar Array Simulator (SAS) is a DC current source with very low output capacitance that can simulate the I-V curve of a solar array under different conditions. The I-V curve is programmable over the GPIB, LAN, and USB interface.

The two PV generators are emulated by two solar array simulators (SAS). The two SAS used are the model E4362A mounted in the mainframe E4360A, all of them manufactured by Keysight. Each SAS has 600 W of maximum power and can be configured as a PV array with 130 V as the maximum open-circuit voltage and 5 A as short-circuit current. [17]

It should be noted that the SAS supports SCPI (Standard Commands for Programmable Instruments) and in this case, the MATLAB software controls the PC supervisory algorithm.

4.1.2. Inverters

The two used inverters (INV) are the model Sunny Boy SB700 manufactured by SMA, and they are configured with 460 W, as rated output power. In general, the Sunny Boy takes power from a DC source (PV modules) and converts it to AC power for the utility grid. Figure 3.11 shows the schematic of the inverter position in the system. [18]

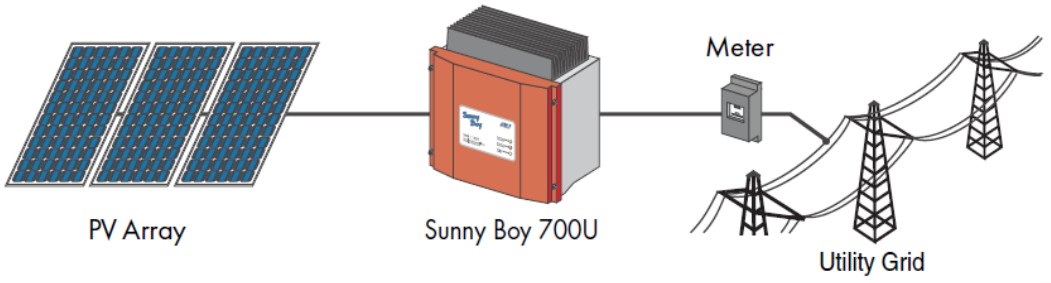

Figure 3.11. Sunny Boy 700U Installed in a Utility Interactive PV System

4.1.3. Arduino

The system controller is based on MATLAB and Arduino UNO as a general-purpose programable platform. This controller monitors the inverter's output power and, in accordance with Equation (3.5), sends the order to the switch to group or divide the PV arrays.

The whole operation of the system is supervised by a personal computer (PC). The PC sets the simulation steps by programming the I-V characteristic curve in each SAS and records the energy delivered to the grid by the inverters.

4.1.4. Relay

The switch used in the system is based on an electromagnetic relay implemented in the D1 Mini Relay Shield, this device is compatible with the products of the Arduino family. A digital input receives the command from Arduino and the status of the system turns to grouping or division. [19]

4.1.5. Power-Meter

Each inverter is connected to the grid through an energy meter (EM) model EM111DINAV81XS1X manufactured by Carlo Gavazzi. This energy meter can measure bidirectional power in 230 V grids with current up to 45 A. [20]

4.1.6. Communication Protocols

Figure 3.12 illustrates the practical implementation of the experimental setup. It involves several connections: one for linking the SAS to the personal computer using GPIB and USB, and others for connecting the energy meters and Arduino UNO controller through RS485 and RS232.

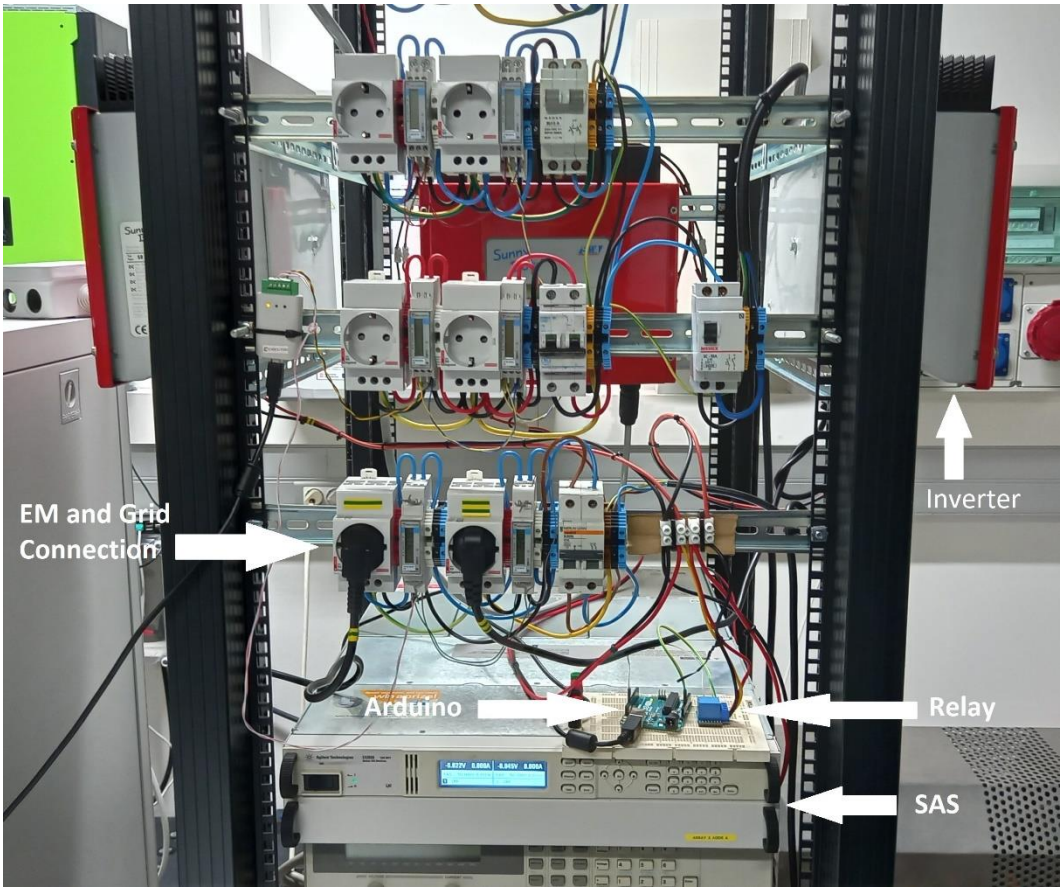

Figure 3.12. The experimental set used for a team-based GCPV system characterization

4.2. Inputs and Outputs

To address potential issues and ensure data accuracy, it is essential to conduct necessary calculations and processing before proceeding to the final stage of the emulation. These steps help mitigate problems and allow for data adjustment as required.

4.2.1. Data Processing

As mentioned in section 2.2, temperature and irradiance should be inserted into the code as input. To simplify the process, the temperature is assumed to be 25 ^{o}C.

In the case of Irradiance, websites such as SoDa [21] offer valuable information based on the desired location. While it is possible to select average irradiance values for different intervals, such as month by month or minute by minute, accessing data at a per-second level is not available. Consequently, data processing is necessary to prepare it for real-time analysis throughout an entire day. To obtain a per-second data set, interpolation is performed as part of the process.

Additionally, it is evident that there are zero values at the start and end of the day. By removing these values, an effort has been made to enhance the simulation speed. In figure 4.1, the irradiance values obtained from SoDa are displayed, reflecting the removal of zero values. On the other hand, figure 4.2 depicts a plot of the interpolated data, illustrating the results after the interpolation process.

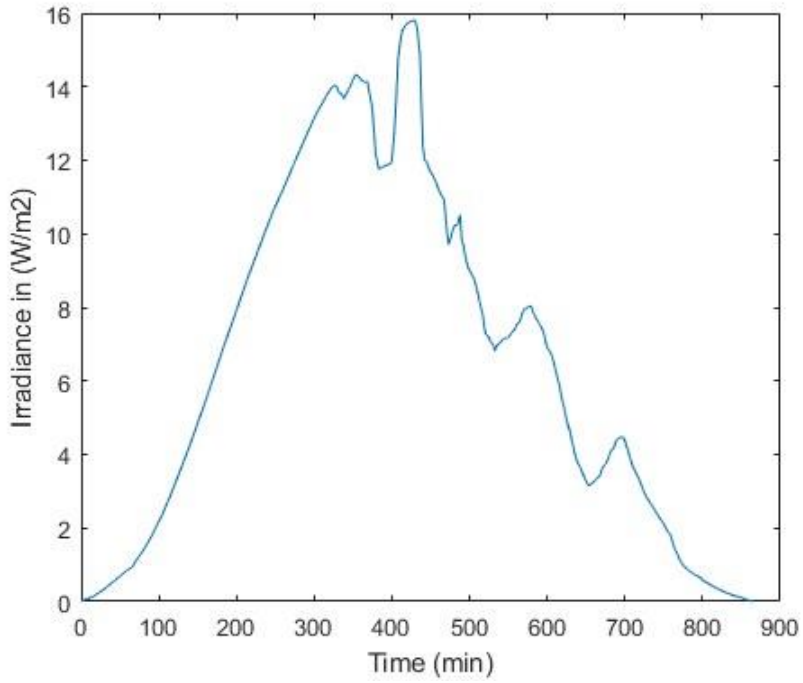

Figure 4.1. The irradiance values per minute, after eliminating the zero values.

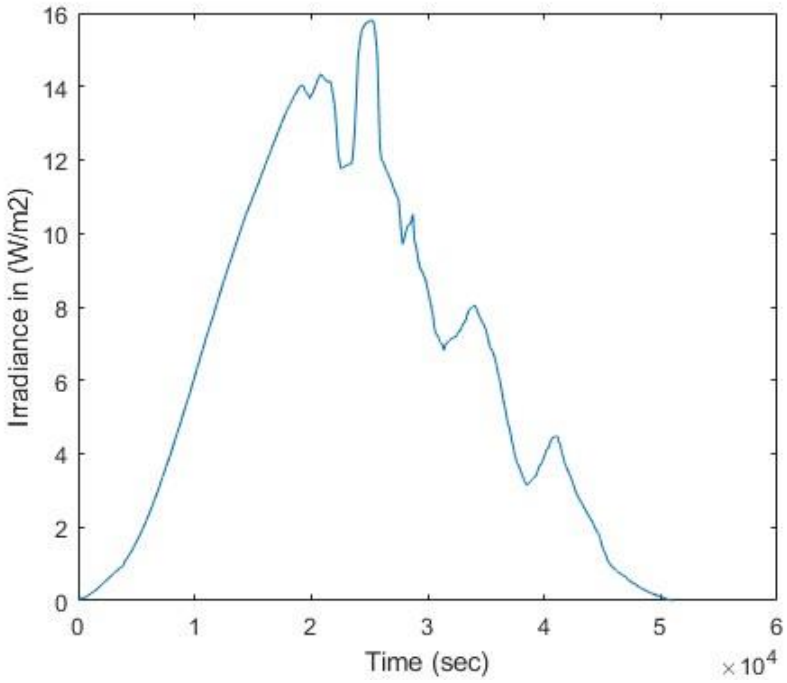

Figure 4.2. The irradiance values per second, after interpolation.

4.2.2. Transient state during switching

In contrast to theoretical assumptions, a certain duration is required for electrical devices to attain a stable state following any change. This section focuses on calculating the time needed to traverse these transient states after switching. Considering this delay in the measurement and control system helps us ignore temporary values and prevent unintended system switching.

Figure 4.3 displays the AC powers delivered by two inverters along with the switch status. It is important to note that the switch status is multiplied by 100 to enhance clarity. After the switching at the 200th second, a division is carried out, assuming the second inverter becomes active. However, as depicted in the figure, it takes approximately 95 seconds for the second inverter to deliver the desired power.

This implies that after the division switching, the control system should wait for approximately 100 seconds before it starts operating. Additionally, there is a power drop, and these switching losses will be presented in the results chapter.

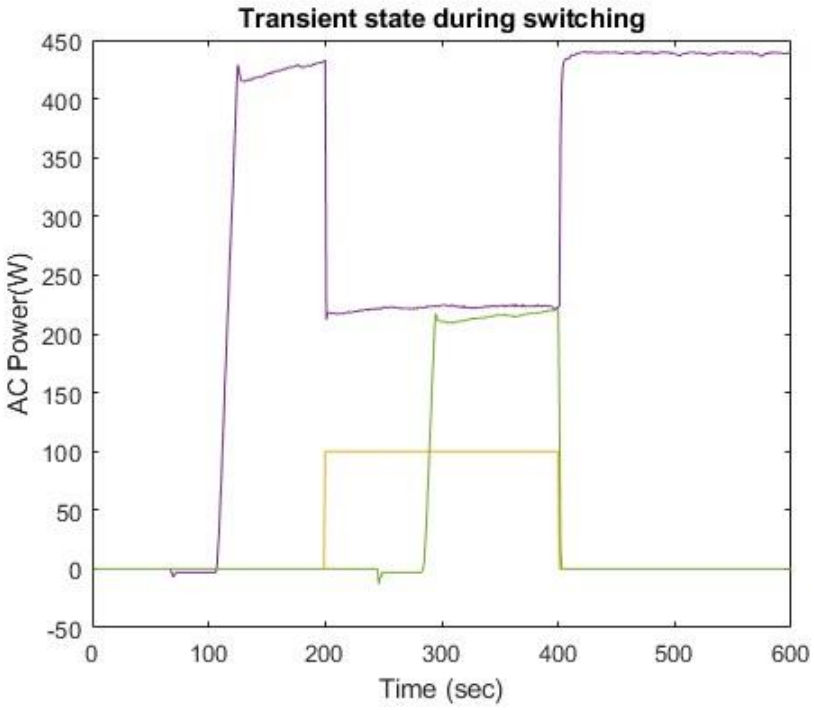

Figure 4.3. AC power delivered by two inverters along with the switch status.

Furthermore, as depicted in figure 4.3, a switching event(grouping) occurs at the 400th second, and in this case, the system responds promptly without any required delay. In summary, figure 4.4 provides an overview of the total AC power.

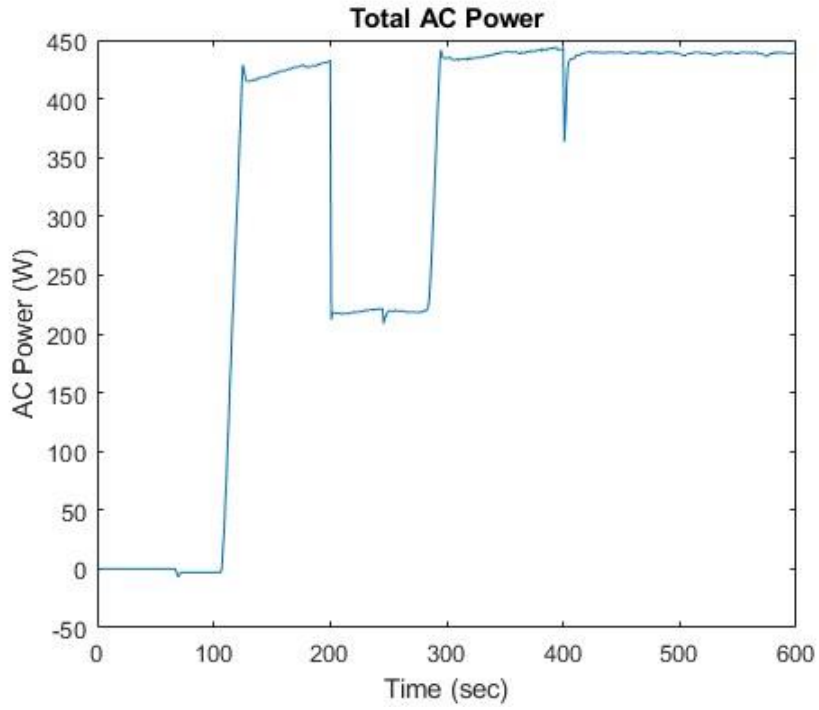

Figure 4.4. Total AC power delivered to the grid.

4.2.3. Threshold Margin

Setting a fixed threshold value can lead to the issue of getting stuck in a switching loop. This problem arises when values slightly above or below the threshold are incorrectly considered as switching points, causing undesired repeated switching.

Figure 4.5 demonstrates this problem with two switching points observed during a sunny day, and one of them is depicted in more detail in Figure 4.6. It is evident that multiple switching has occurred within a short period of time. Figure 4.7 exhibits the same problem on a partly sunny day, highlighting the occurrence of multiple switching.

In order to address this issue, defining a margin or hysteresis is proposed. In this regard, instead of using a specific value, the switching logic considers an upper limit and a lower limit. For instance, in our case, the lower power is 90 watts and the higher one is 105 watts. The results presented in Chapter 5 provide evidence that this method is indeed effective and useful.

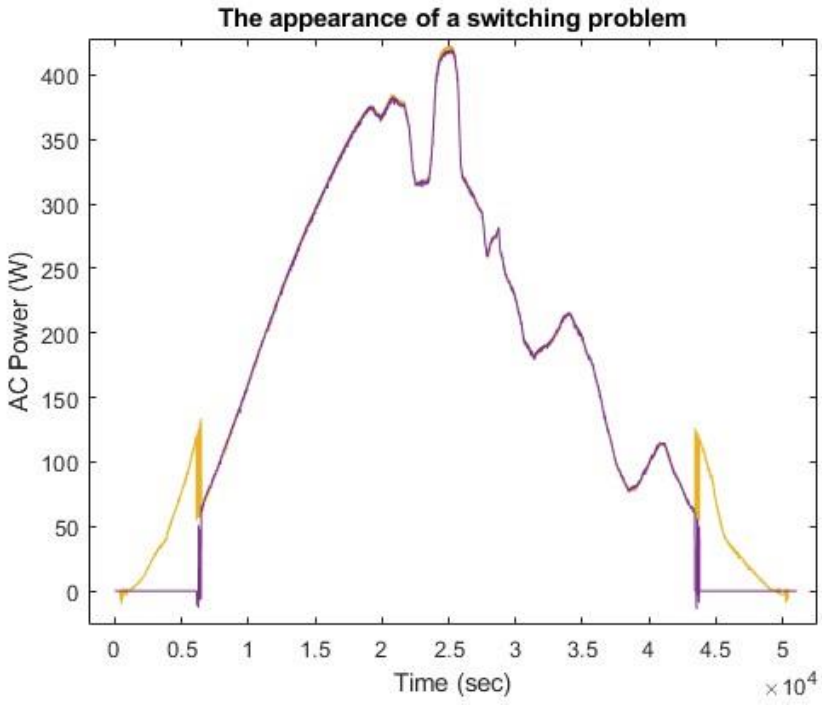

Figure 4.5. Multiple switching problem during the emulation of a sunny day.

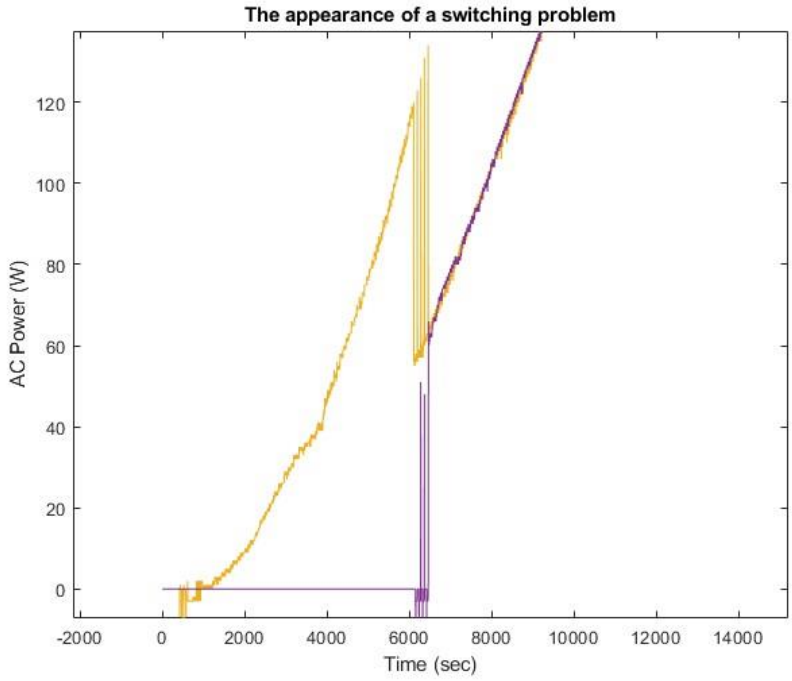

Figure 4.6. Multiple switching problem.

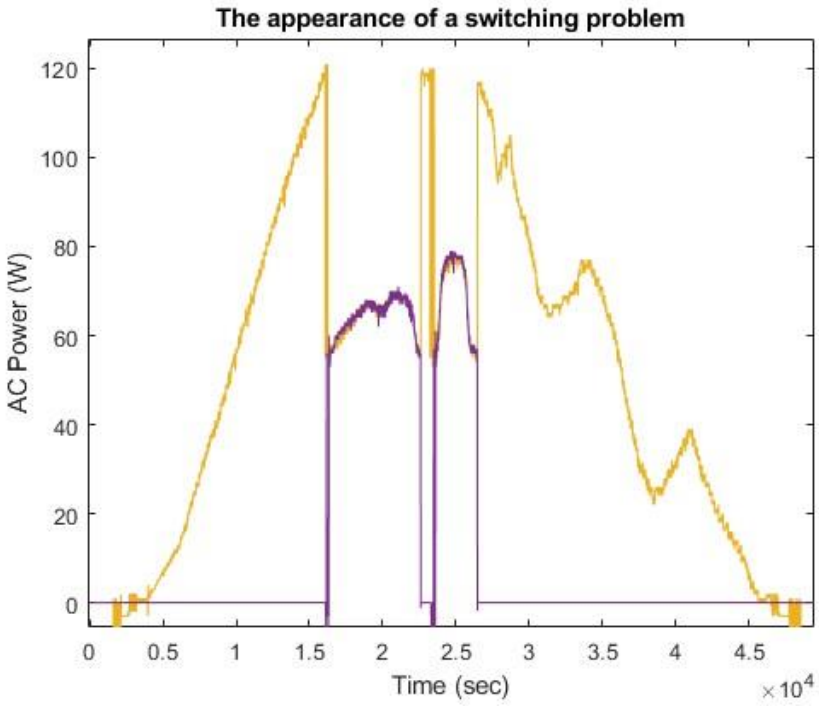

Figure 4.7. Multiple switching problem during the emulation of a partly sunny day.

4.2.4. Energy Calculation

The following chapter covers the simulation and comparison of fixed and reconfigurable systems. In order to determine the preferred system, a reliable criterion is needed. In our study, the energy delivered to the grid is regarded as the key determining factor. Since the input data set is similar in each case, the higher output can be interpreted as indicating higher efficiency. Equation (4.1) describes the method for calculating this energy.

$$E_{grid} = \int_0^T P_{AC}(t) \, . \, dt \qquad \textbf{(Eq. 4.1)}$$

5. Results

In this chapter, both a fixed system and a reconfigurable system are emulated under sunny, cloudy, and partly sunny conditions. The objective of this section is to evaluate and compare the performance of these systems.

5.1. Sunny Day

A sunny day is distinguished by the typical rise and set of the sun, free from the presence of clouds. As a result, the irradiance level can reach higher values, and typically only two switching actions are required. The first action involves division when the irradiance reaches the threshold, while the second action involves grouping when the power reduces and drops below the threshold.

As depicted in Figure 5.1, the fixed system employs two parallel inverters. Similarly, as previously demonstrated in Figure 3.8, team systems have the flexibility to choose between operating with one or two inverters.

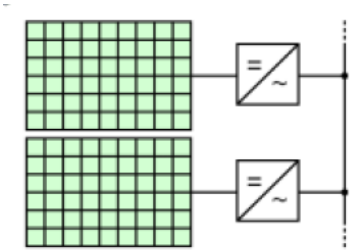

Figure 5.1. Configuration of the fixed system.

5.1.1. Fixed System

Figure 5.2 illustrates the AC powers flowing through the inverters to the grid, while Figure 5.3 represents the total AC power. Generated power during the day follows the same pattern as irradiance, as expected.

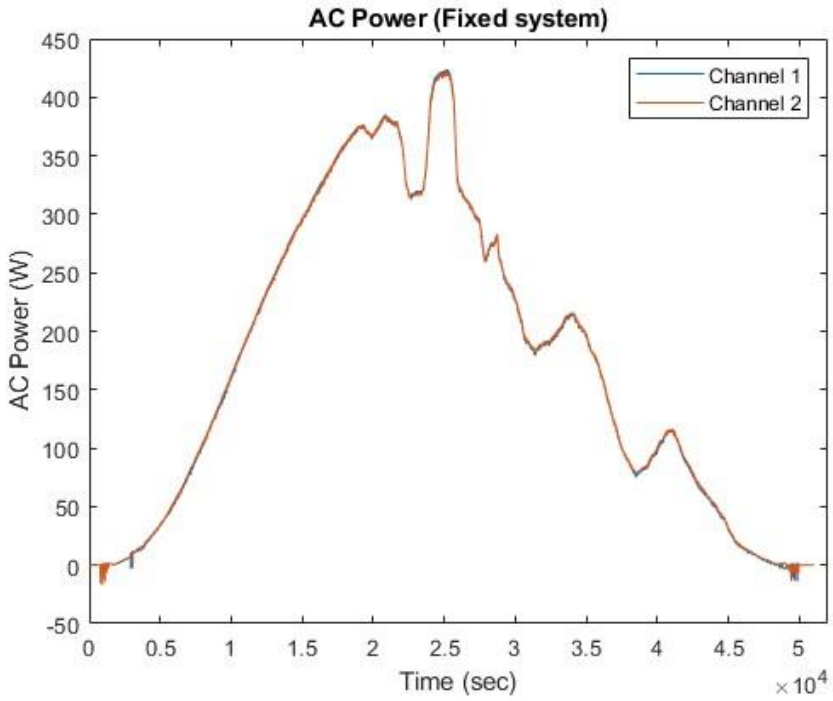

Figure 5.2. AC power delivered by two inverters.

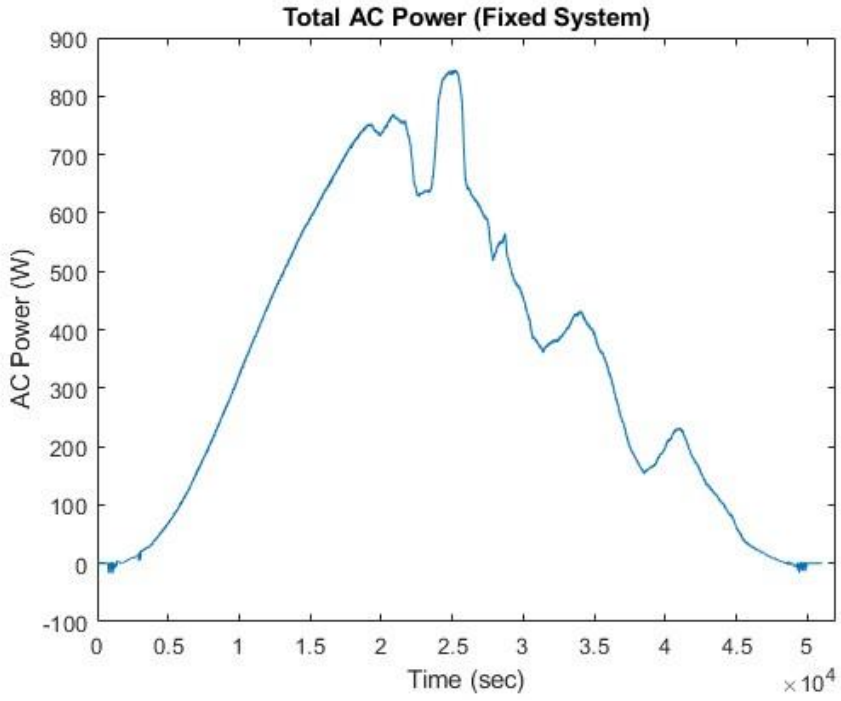

Figure 5.3. Total AC power delivered to the grid.

5.1.2. Configurable System

As depicted in Figure 5.4, initially one of the inverters is utilized. However, once the threshold is reached, the second inverter is added (division). At the end of the period, when the power is lower than the threshold, the reverse action of grouping takes place.

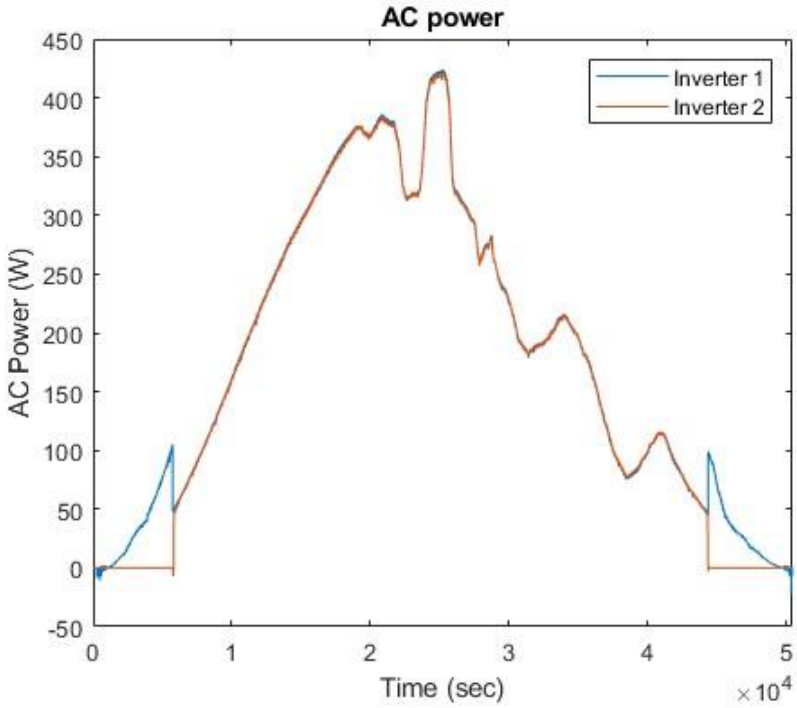

Figure 5.4. AC power delivered by two inverters.

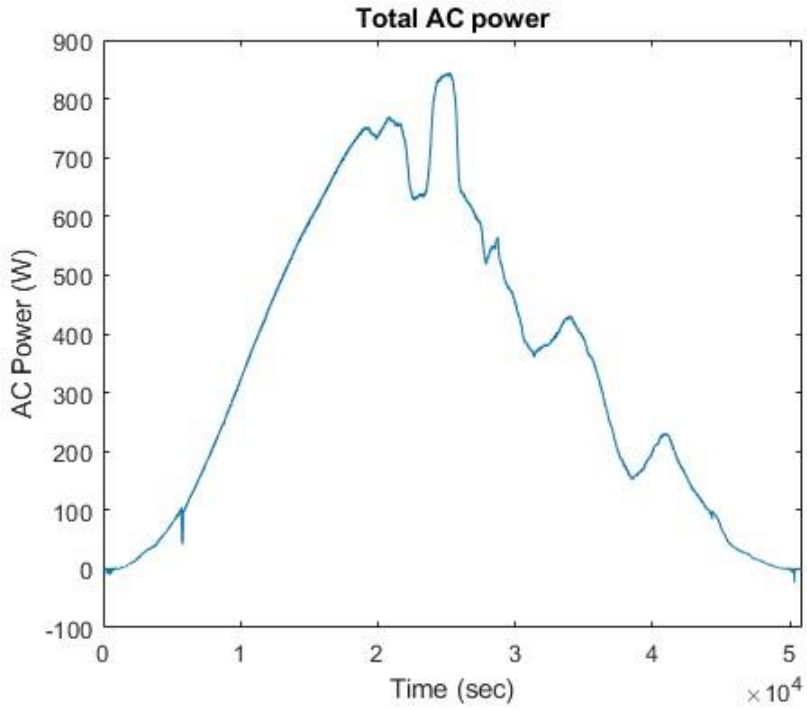

Figure 5.5. Total AC power delivered to the grid.

A small drop at the first switching point can be observed in the total AC power, as shown in Figure 5.5. This loss occurs due to the delay in adding the second inverter. The amount of energy in this period is calculated in the next section (table 5.1).

5.1.3. Comparison

As can be observed in figure 5.6, the fixed and the team system represent different performances in two regions where in both the power is lower than the threshold. During this period, the configurable system operates with a single inverter, and the fixed system works with two parallel inverters. For a more detailed depiction of these areas, refer to Figures 5.7 and 5.8.

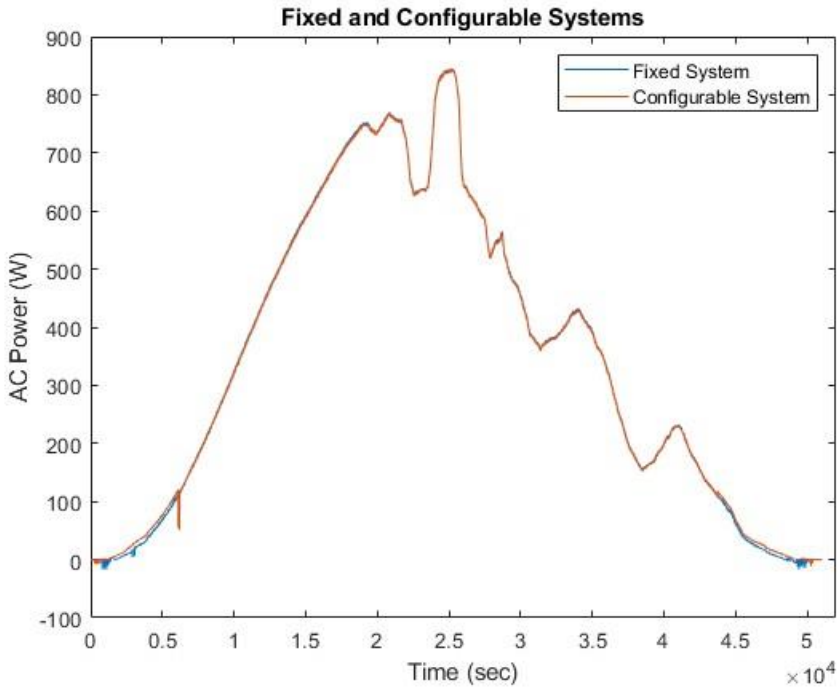

Figure 5.6. AC power delivered by fixed and team system.

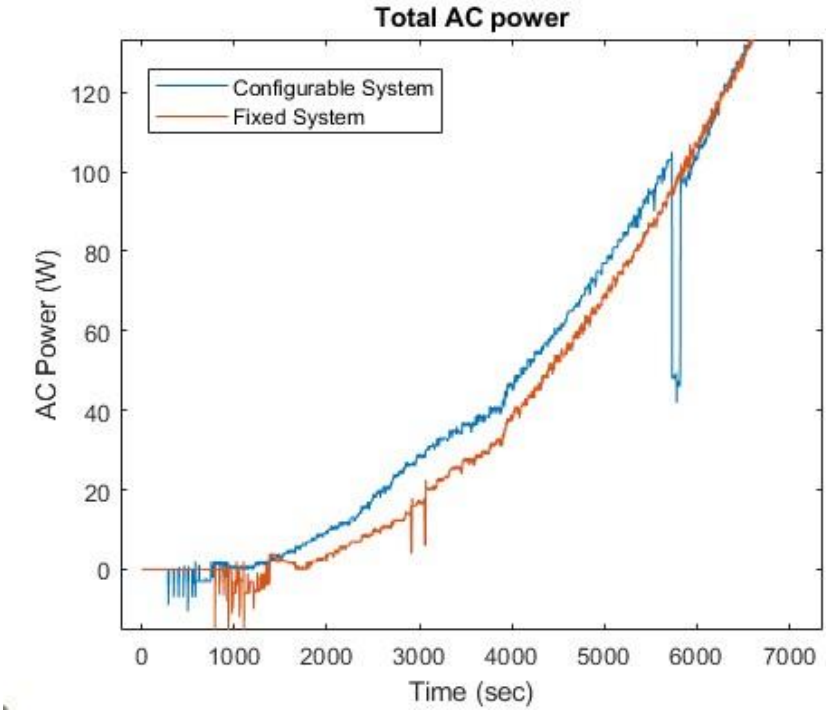

Figure 5.7. The performance difference between the two systems, emphasizing the heightened clarity.

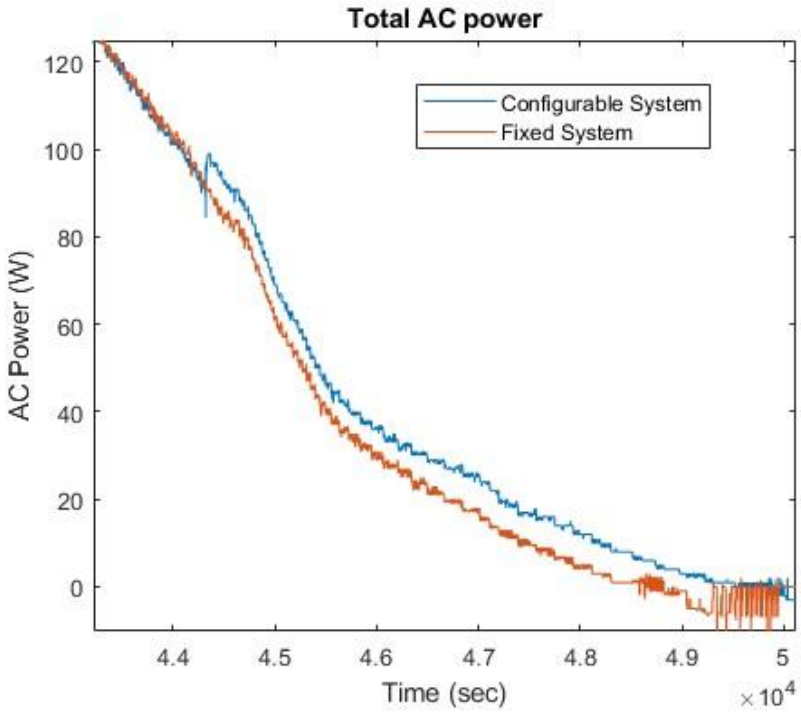

Figure 5.8. The performance difference between the two systems, emphasizing the heightened clarity.

Moreover, based on equation (4.1), the energies delivered to the grid are calculated and presented in table 5.1. As discussed in the previous section, the last column represents the energy left out of generation during switching.

	Energy delivered by first inverter (kWh/day)	*Energy delivered by second inverter (kWh/day)*	*Total delivered energy (kWh/day)*	*Energy reduction during switching (kWh/switching)*
Fixed system	*2.427759*	*2.431556*	*4.859315*	---
Team system	*2.487432*	*2.386352*	*4.873784*	*0.0011*

Table 5.1. Calculated energies comparison according to two systems.

It is obvious that the team system generated slightly more power than the fixed system. Although it has losses, overall delivered power is around 0.014469 (kWh/day) higher.

5.2. Cloudy Day

In this study, a cloudy day is defined as a day in which, due to various factors including cloudiness, the amount of radiation is at such a low level that the power delivered by the system does not reach the threshold.

5.2.1. Fixed System

Figure 5.9 displays the delivered power by inverters and as expected they operate at almost the same level of power. Additionally, figure 5.10 shows the total AC power that is always under the threshold level.

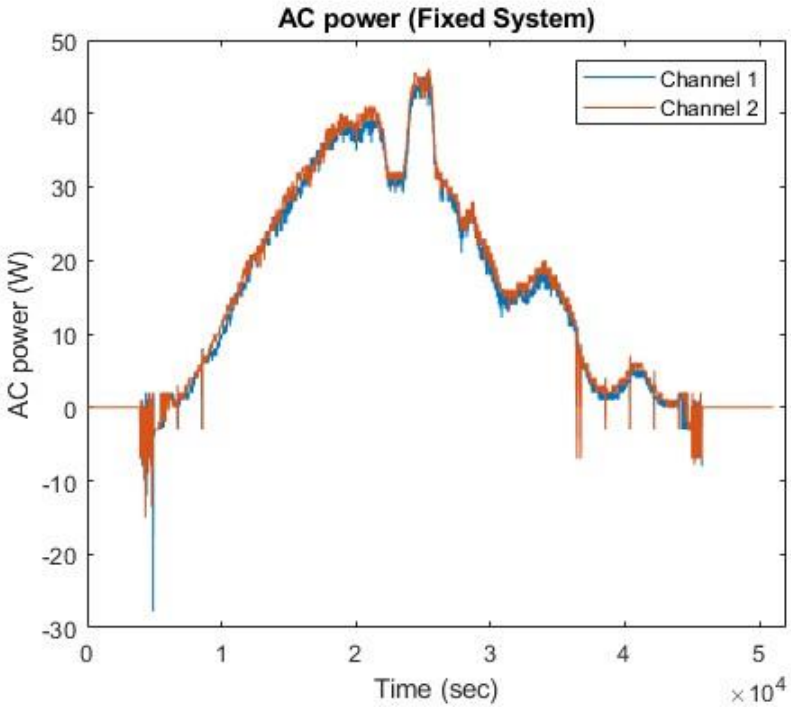

Figure 5.9. AC powers delivered by two inverters**.**

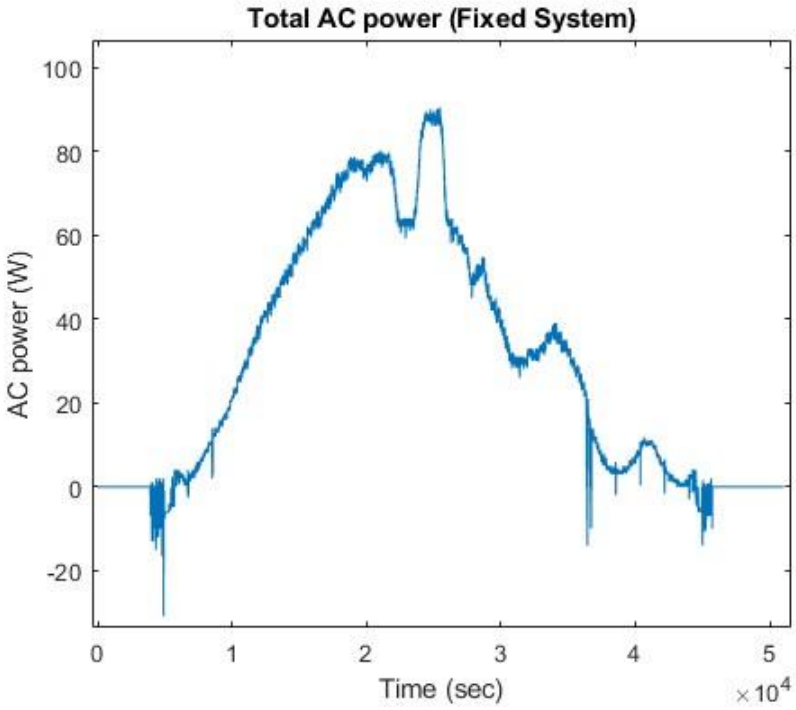

Figure 5.10. Total AC power delivered to the grid**.**

5.2.2. Configurable System

Figure 5.11 proves that the configurable system utilizes one inverter during the whole day to increase the efficiency of the system, and it Reminds the fact that when the generation is at a low level, a higher sizing ratio can be helpful to increase the efficiency. The total AC power delivered to the grid is displayed in figure 5.12 and it is clear that all power flows through the first inverter.

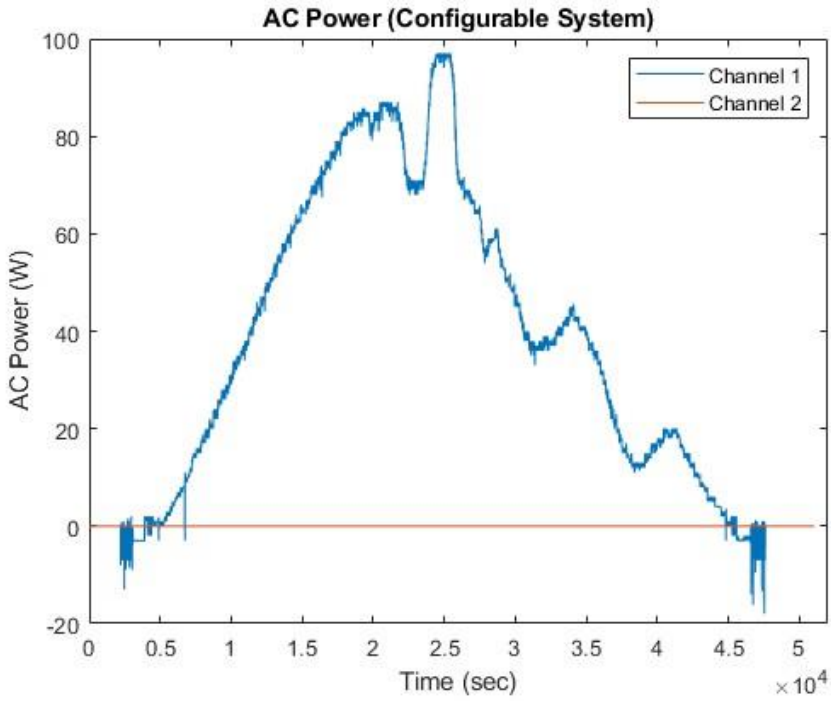

Figure 5.11. AC power delivered by two inverters**.**

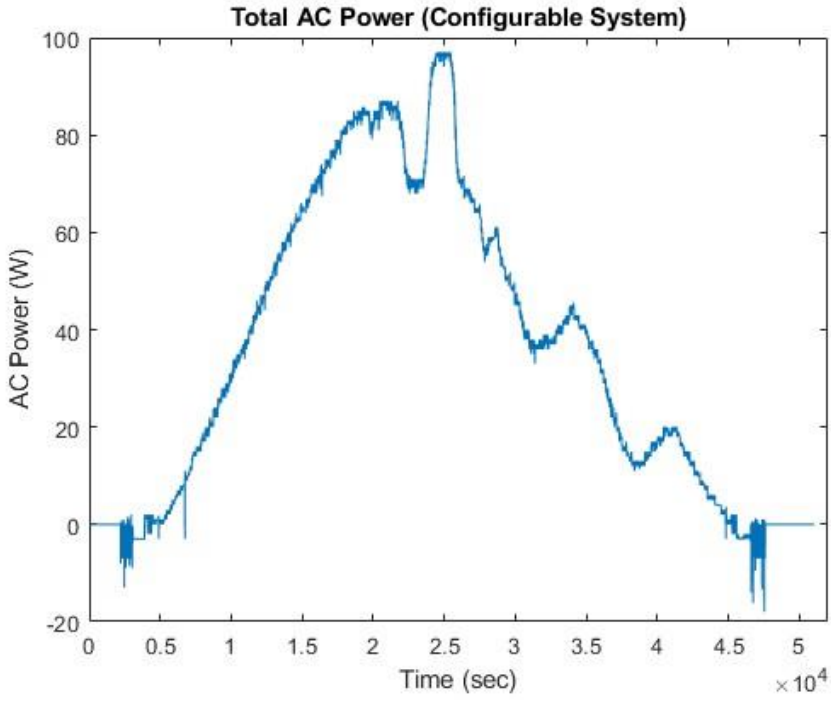

Figure 5.12. Total AC power delivered to the grid**.**

5.2.3. Comparison

In order to make a comparison, AC powers of both systems are shown in figure 5.13. As expected, the configurable system delivers a higher level of power during the day.

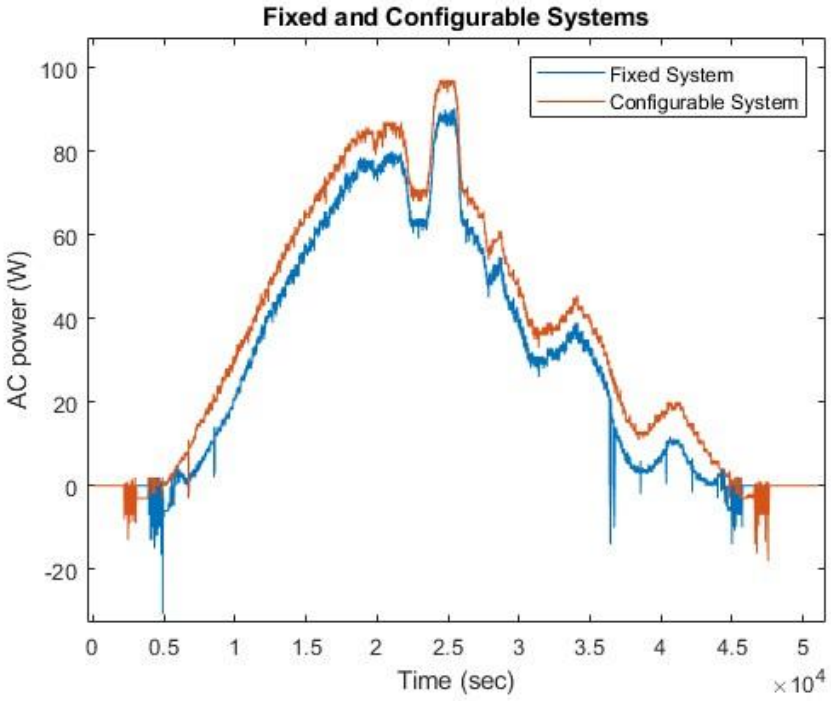

Figure 5.13. AC power delivered by fixed and team system.

In addition, the energies delivered to the grid are calculated and presented in Table 5.2. Referring to the obtained results, it can be concluded that on a cloudy day, the configurable system demonstrates a more significant deviation (0.088799 (kWh/day)).

	Energy delivered by first inverter (kWh/day)	*Energy delivered by second inverter (kWh/day)*	*Total delivered energy (kWh/day)*	*Energy reduction during switching (kWh/switching)*
Fixed system	*0.201245*	*0.210009*	*0.411254*	---
Team system	*0.500053*	*0*	*0.500053*	---

Table 5.2. Calculated energies comparison according to two systems.

5.3. Partly Sunny Day

In this study, a partly sunny day is defined as a day in which, due to various factors, the amount of radiation fluctuates, resulting in the power delivered by the system surpassing or falling below thresholds multiple times. Consequently, on a partly sunny day, configurable systems perform more switching compared to sunny days.

5.3.1. Fixed System

The fixed system shows its typical behavior again by following the irradiance pattern and connecting to the grid with two inverters. Figure 5.14 displays AC powers delivered by inverters and while figure 5.15 depicts the total AC power.

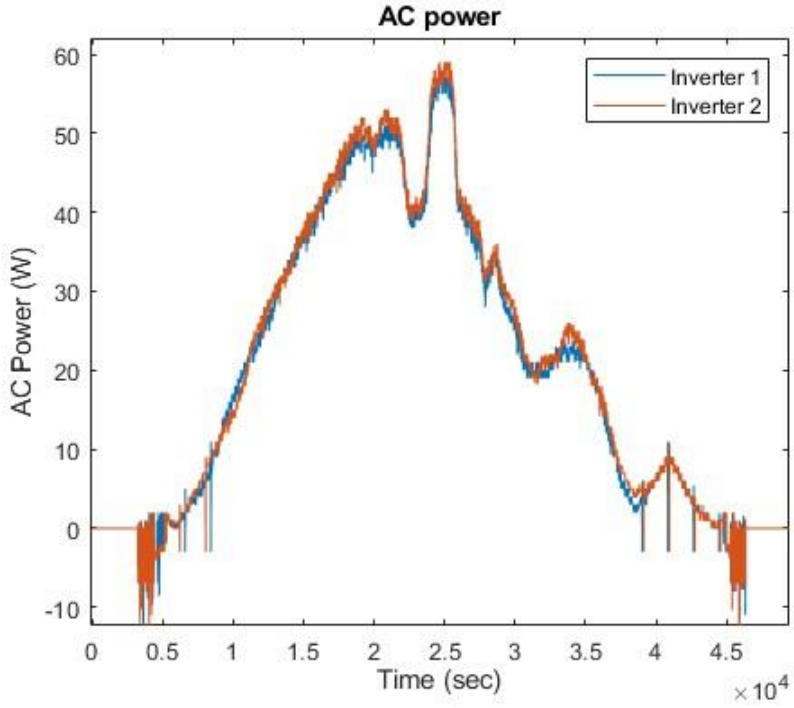

Figure 5.14. AC power delivered by two inverters**.**

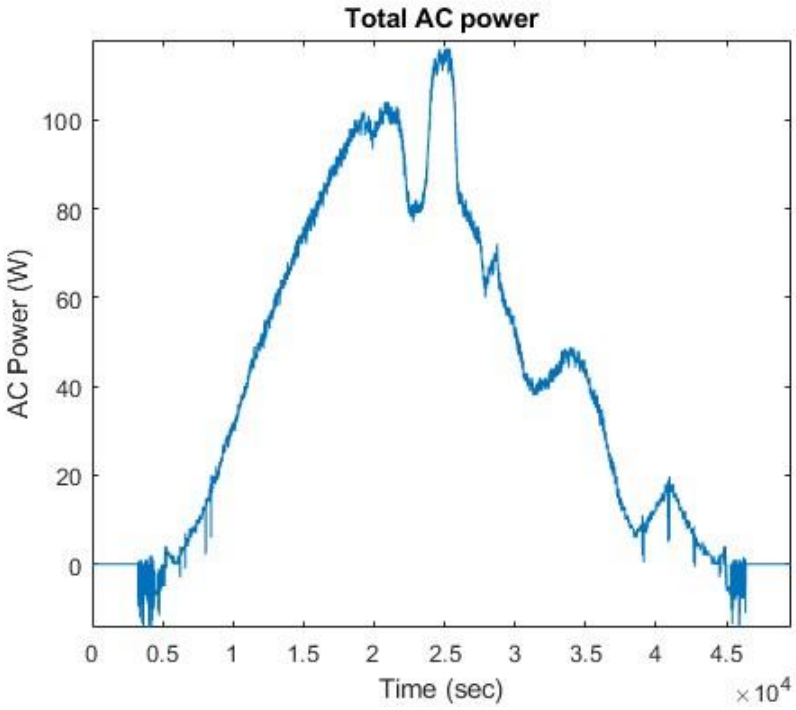

Figure 5.15. Total AC power delivered to the grid**.**

5.3.2. Configurable System

As expected, this case includes several switching, and figure 5.16 shows the effect of these switching on the AC power of inverters. According to the figure, the switching action has occurred four times. Based on the conditions, the second inverter is added to the circuit in two stages and subsequently removed.

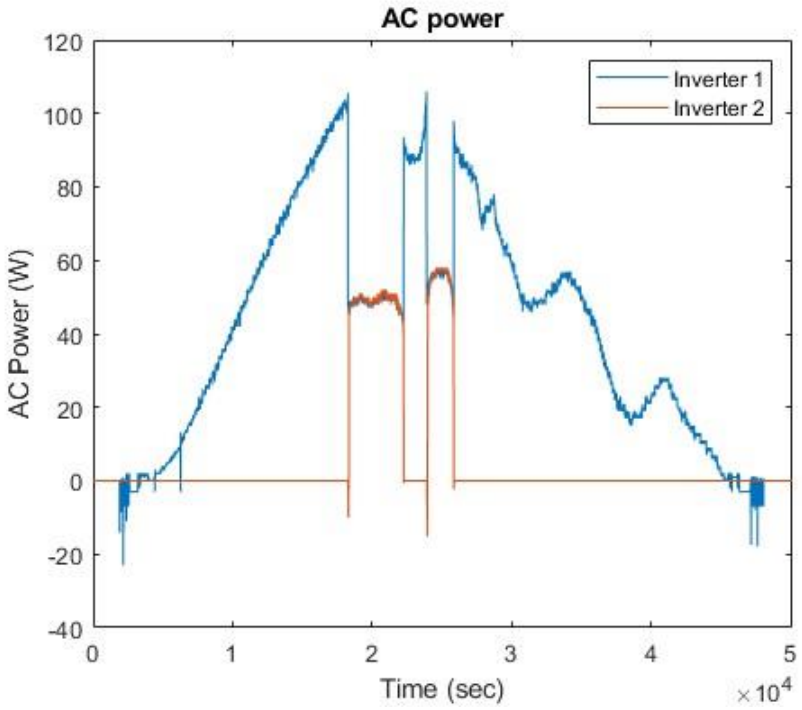

Figure 5.16. AC power delivered by two inverters**.**

The total AC power delivered to the grid and the switch status are shown in Figure 5.17, while the switch status is multiplied by 20 to enhance clarity. It is worth noting that power drops occur at the switching points, particularly those related to division. The amount of energy during this period has been calculated and is presented in the following section (Table 5.3).

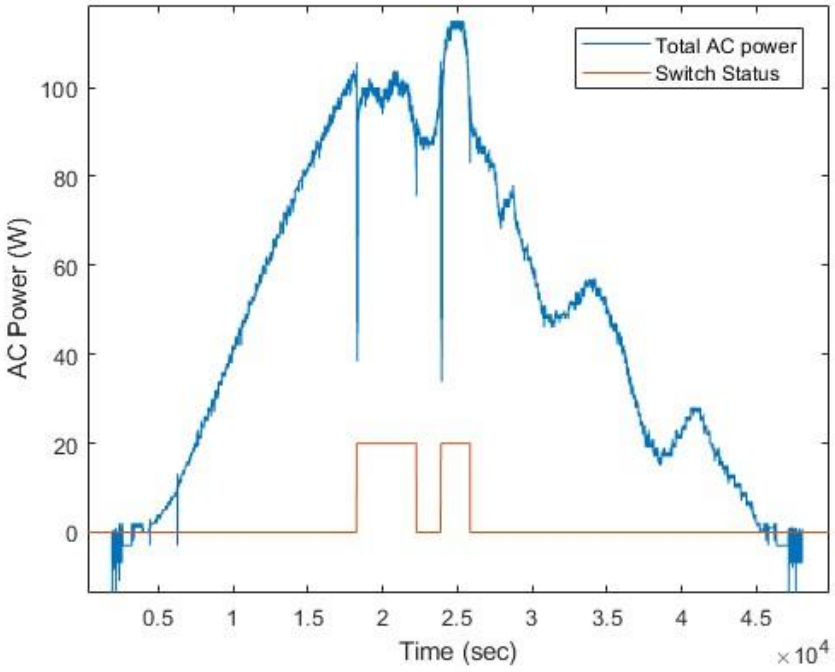

Figure 5.17. Total AC power delivered to the grid and the switch status**.**

5.3.3. Comparison

Figure 5.18 represents a comparison of two systems in terms of delivered AC power. Similarly, the configurable system demonstrates better performance in sections below the threshold.

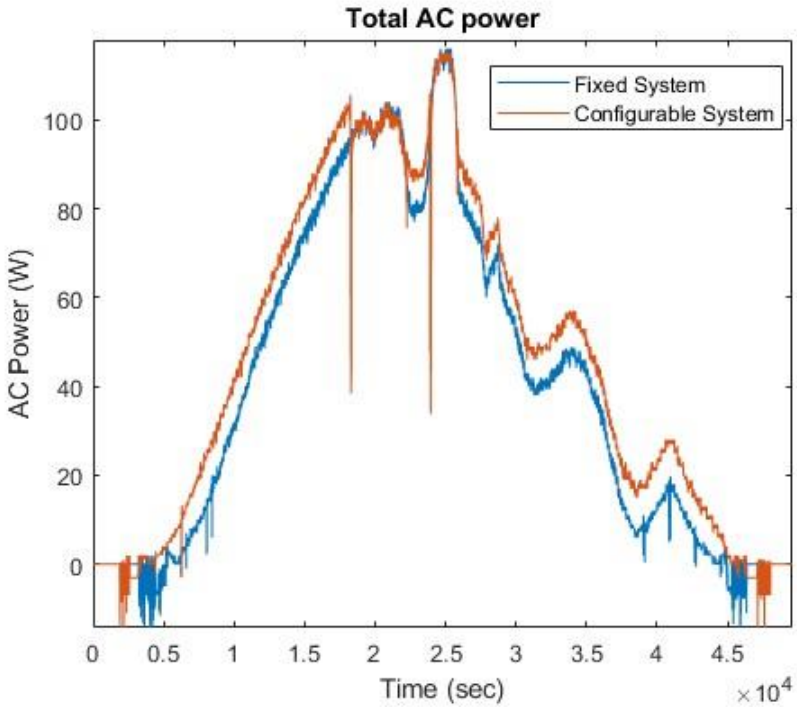

Figure 5.18. AC power delivered by fixed and team system.

Moreover, the energies delivered to the grid are calculated and presented in Table 5.3. Although the difference between the two systems in delivered energy is not as high as a cloudy day, it is still significant (0.077226 (kWh/day)). However, the last column of the table reveals higher amounts of energy reduction due to the increased number of switching actions.

	Energy delivered by first inverter (kWh/day)	*Energy delivered by second inverter (kWh/day)*	*Total delivered energy (kWh/day)*	*Energy reduction during switching (kWh/switching)*
Fixed system	*0.271999*	*0.279582*	*0.551581*	---
Team system	*0.546445*	*0.082363*	*0.628807*	*0.0021*

Table 5.3. Calculated energies comparison according to two systems.

5.4. General comparison

Table 5.4 provides an overview of the results obtained from previous emulations. The fixed system operates with two inverters, which means that our basic configuration is based on two inverters. In

contrast, the configurable system offers the flexibility to utilize a single inverter during low-power periods, therefore, being in these operational areas is decisive and leads to changes. The results presented in table 5.4 validate this theory, showing that days with lower power levels demonstrate greater increases in delivered energy when utilizing the configurable system.

	Sunny day	*Cloudy day*	*Partly sunny day*
Increment of energy (kWh/day)	*0.014469*	*0.088799*	*0.077226*
Energy Gain	*0.2977%*	*21.59%*	*14.0%*

Table 5.4. Increase in the amount of energy delivered to the grid and energy gains.

In this regard, a notable variation observed on cloudy and partly sunny days suggests that it would be advisable to employ team systems in regions characterized by low average radiation or low power levels.

On the contrary, a minor change in the results of the sunny day emulation can be interpreted to indicate that utilizing the team system in locations with very high average radiation does not significantly impact the efficiency.

5.5. Effect of threshold

According to table 3.2, the utilization of merged or cleaned data results in distinct threshold values. Moreover, as mentioned in section 4.2.3, in order to determine the threshold, it is necessary to consider a margin to avoid switching problems. Since the threshold can affect the efficiency of the system, a practical method of selecting this margin can be considered. However, in this section, a comparison is presented to demonstrate the impact of different margins on the delivered energy.

Table 5.5 provides valuable information regarding the selected margins and energy gain obtained from two datasets and the emulation conducted on sunny and partly sunny days. Since there is not any switching on cloudy days, adding it to the table is useless.

		Threshold margin	*Energy gain*
Sunny day	*Merged data*	*(110-125)*	*0.1976%*
	Cleaned data	*(90-115)*	*0.2977%*
		(95-110)	*0.3164%*
Partly sunny day	*Merged data*	*(110-125)*	*8.369%*
	Cleaned data	*(90-115)*	*14.0%*
		(95-110)	*14.72%*

Table 5.5. Selected margins and energy gains.

The selection of the margin offers various possibilities, such as adjusting the width and position. Two margins are chosen based on the threshold derived from cleaned data. In one scenario, the threshold point is precisely positioned in the middle of the band, while in the other, it is located closer to the border.

Based on the information presented in table 5.5, it is evident that utilizing the cleaned data results in a more appropriate threshold selection. Additionally, positioning the threshold in the middle of the band proves to be advantageous in terms of achieving better energy gain.

6. Conclusions

The focus of this master's thesis was on fixed and team systems, which are grid-connected PV configurations. In order to analyze and compare their energy efficiency, a configurable system was designed by establishing a model and conducting relevant calculations. Furthermore, several emulations were performed to assess the performance of these systems.

The results obtained from these emulations demonstrate that the configurable system exhibits superior performance on cloudy and partly sunny days. However, on sunny days, a slight variation in the delivered energy is observed.

Furthermore, a series of emulations were conducted to evaluate the impact of different threshold margins on energy gain. The outcomes of these tests emphasize that utilizing a threshold margin obtained from cleaned data and placing the calculated threshold in the center leads to the highest values of energy gain.

Given the findings of this study, it would be worthwhile for future research to focus on determining the optimal margin that can maximize energy gain. Exploring different methodologies and approaches to identify the most suitable margin could contribute to further enhancing the performance and efficiency of grid-connected PV systems.

7. Economic analysis

The project's primary costs encompass software, hardware, and human resources. Table 7.1 provides an estimated total of these expenses. It is important to highlight that certain costs have been adjusted using a coefficient, resulting in only a portion of their original price being accounted for in this project.

		Unit/Hour	*Price (€)*	*Percentage of use*	*Cost (€)*
Software	*MATLAB*	*1*	*860*	*5%*	*43*
	Microsoft 365	*1*	*69*	*5%*	*3.45*
Hardware	*Inverters*	*2*	*800*	*5%*	*80*
	PC	*1*	*1000*	*5%*	*50*
	SAS	*1*	*24000*	*5%*	*1200*
human resources	*Engineer*	*80*	*80*	*100%*	*6400*
	Auxiliary	*520*	*40*	*100%*	*20800*
				Total	*28576.45*

Table 7.1. Estimation of the project costs

Project costs (€)	*28576.45*
Non-direct costs (5%) (€)	*1428.82*
Total (€)	*30005.27*

Table 7.2. Estimation of the project costs

Furthermore, a specific amount is designated for indirect costs in the project budget. The estimated amount for these costs can be found in table 7.2, which is calculated based on the total project cost, and the final project cost is determined by incorporating this amount into the total cost calculation.

Reference

[1] IEA (2023), Renewable Energy Market Update -June 2023, IEA, Paris https://www.iea.org/reports/renewable-energy-market-update-june-2023, License: CC BY 4.0

[2] "EU Solar Energy Strategy". European Commission, Department of Energy. Brussels, May 2022. Available online at: https://eur-lex.europa.eu/legal-content/EN/TXT/?uri=COM%3A2022%3A221%3AFIN&qid=1653034500503

[3] IRENA (2023), Low-cost finance for the energy transition, International Renewable Energy Agency, Abu Dhabi. Available online at: https://www.irena.org/Publications/2023/May/Low-cost-finance-for-the-energy-transition

[4] Velasco, G.; Martinez, H. "Sizing Factor Considerations of Grid-Connected Photovoltaics Systems". In: "Solar Energy Systems: Progress and Future Directions". New York: Nova Science Publishers, Inc., 2019, p. 61-101. ISBN: 978-1-53616-142-7

[5] Camps, X., Velasco, G., de la Hoz, J. and Martín, H. "Contribution to the PV-to-inverter Sizing Ratio Determination Using a Custom Flexible Experimental Setup". Applied Energy 149: 35-45 (2015), doi:10.1016/j.apenergy.2015.03.050

[6] Burger, B.; Rüther, R. "Inverter Sizing of Grid-connected Photovoltaic Systems in the Light of Local Solar Resource Distribution Characteristics and Temperature". Solar Energy, Vol. 80, No. 1: 32-45. (2006). doi:10.1016/j.solener.2005.08.012

[7] Skoplaki, E.; Palyvos, J. A. "Operating Temperature of Photovoltaic Modules: A Survey of Pertinent Correlations". Renewable Energy, 34, no. 1: 23-29. (2009). doi:10.1016/j.renene.2008.04.009.

[8] Nordmann, T.; Clavadetscher, L. "Understanding temperature effects on PV system performance". Proceedings of the 3rd WCPEC: 2243-2246. Osaka (May 2003)

[9] G. Velasco, F. Guinjoan, R. Piqué, M. Román, A. Conesa. "Simulation-based criteria for the power sizing of grid-connected PV systems". International Review on Modelling and Simulations (I.RE.MO.S.), Vol. 4, N. 5 (2011)

[10] Mühlberger, T.; Wolfahrt, J. "Modular System. Maximum Yield: Fronius MIXTM System Optimizes Yield". Fronius International GmbH, photovoltaic system technology (2012)

[11] "Utility Scale Solar Inverters". Emerson Electric Co. (2013). P.N. 0701-0006-14 10/13

[12] "ABB central inverters. ULTRA-750/1100/1500 - 750kW to 1560kW". ABB (2015). Available online at: https://www.fimer.com/sites/default/files/ULTRA-EN-Rev%20E.pdf

[13] "Vacon 8000 solar inverter. A driving force in solar energy". Vacon (2012). DPD01502G

[14] Jasper, A., Blume, L. and Glowka, M. "Sunny Family 2008/2009". SMA Solar Technology AG (2008).

[15] "Central inverter SUNNY CENTRAL User Manual". SMA Solar Technology AG (2020). Available online at: https://files.sma.de/downloads/SC-BEN092751.pdf

[16] Baumgartner, F. P.; Schmidt, H.; Burger, B.; Bründlinger, R.; Häberlin, H.; Zehner, M. "Status and Relevance of the DC Voltage Dependency of the Inverter Efficiency". Proceedings of the 22nd EU PVSEC. Milan (September 2007)

[17] KEYSIGHT TECHNOLOGY. Series E4360 Modular Solar Array Simulator (2018). Available online at: https://www.keysight.com/es/en/product/E4362A/solar-array-simulator-dc-module-130v-5a-600w.html.

[18] Sunny Boy SB 700U. Installation Guide. Available online at: https://files.sma.de/downloads/SB700U-11-SE3207.pdf

[19] Relay Shield. Available online at: https://www.wemos.cc/en/latest/d1_mini_shield/relay.html

[20] C.GAVAZZI. Energy Analyzer, Type EM111. Available online at: https://www.gavazziautomation.com/images/PIM/DATASHEET/ENG/EM111%20DS%20ENG%20170616.pdf

[21] https://www.soda-pro.com/

Annex A: **SB700 - Data Sheet**

Sunny Boy SB 700

El inversor String

Inversor profesional adecuado también para instalaciones pequeñas

3 rangos distintos de tensión de entrada

SMA grid guard® 2: Conmutador de desconexión automático

Diagnóstico y comunicación a través de la red o por radio-transmisión, así como por cable (RS232 o RS485)

Rango de temperatura ampliado de –25 °C a +60 °C

Indicado tanto para montaje interior como exterior

La tecnología String desarrollada por SMA representa en la actualidad lo más avanzado en materia de instalaciones fotovoltaicas. La separación del generador solar en varios Strings de módulos independientes, asignados a un inversor cada uno, facilita enormemente la instalación y reduce notablemente los costes.
La posibilidad de configurar el rango de la tensión de entrada permite adaptar el SB 700 a las necesidades particulares de cada instalación con unas pocas modificaciones. Eso permite la realización incluso de instalaciones pequeñas conforme al estado actual de la técnica. La tecnología innovadora que emplea el SB 700 garantiza un rendimiento energético óptimo de toda la instalación fotovoltaica.

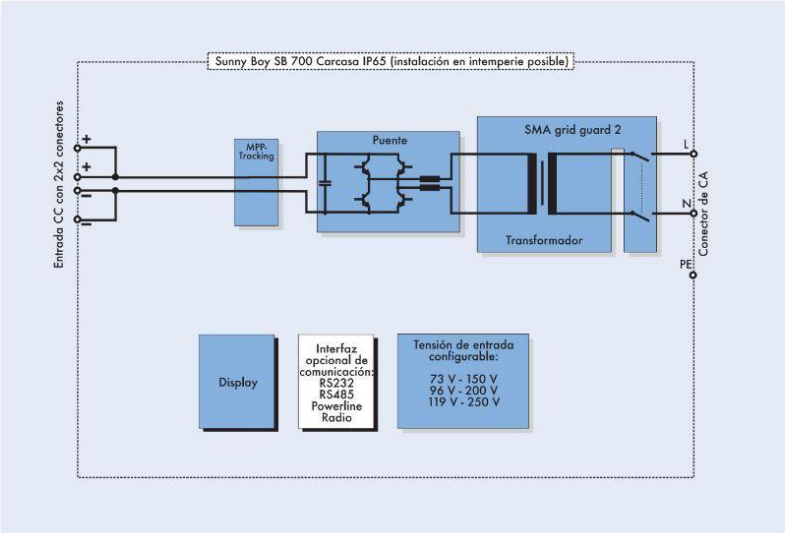

Representación esquemática del Sunny Boy SB 700

Datos Técnicos

	SB 700 (73 a 150 V)	SB 700 (96 a 200 V)	SB 700 (119 a 250 V)
Parámetros de entrada			
Potencia máx. de CC ($P_{CC, max}$)	510 W	670 W	780 W
Tensión máxima de CC ($U_{CC, max}$)	250 V	250 V	250 V
Rango de tensión fotovoltaica, MPPT (U_{FV})	73 V - 150 V	96 V - 200 V	119 V - 250 V
Corriente máx. de entrada ($I_{FV, max}$)	7 A	7 A	7 A
Factor de distorsión de CC (U_{pp})	< 10 %	< 10 %	< 10 %
Número máx. de Strings (en paralelo)	2	2	2
Dispositivo separador de CC	Conector	Conector	Conector
Varistores con control térmico	sí	sí	sí
Monitorización de toma a tierra	sí	sí	sí
Protección contra polarización inversa	Diodo de cortocircuito	Diodo de cortocircuito	Diodo de cortocircuito
Parámetros de salida			
Potencia máx. de CA ($P_{CA, max}$)	460 W	600 W	700 W
Potencia nominal de CA ($P_{CA, nom}$)	460 W	600 W	700 W
Coeficiente de distorsión harmónica (THD)	< 3 %	< 3 %	< 3 %
Tensión nominal de CA ($U_{CA, nom}$)	220 V - 240 V	220 V - 240 V	220 V - 240 V
Frecuencia nominal de CA ($f_{CA, nom}$)	50 Hz / 60 Hz	50 Hz / 60 Hz	50 Hz / 60 Hz
Ángulo de desplazamiento de fase (cos φ)	1	1	1
Resistencia al cortocircuito	sí, regulación de corriente	sí, regulación de corriente	sí, regulación de corriente
Conexión a red	Conector de CA	Conector de CA	Conector de CA
Coeficiente de rendimiento			
Coeficiente de rendimiento máx.	93,4 %	93,4 %	93,4 %
Rendimiento europeo	92 %	92 %	92 %
Grado de protección			
según DIN EN 60529	IP65	IP65	IP65
Parámetros mecánicos			
Ancho / alto / fondo (mm)	322 / 290 / 180	322 / 290 / 180	322 / 290 / 180
Peso	16 kg	16 kg	16 kg

Annex B: Performance Specifications of SAS

Performance Specifications for Keysight E4361A and E4362A SAS Modules

Unless otherwise noted, specifications are warranted over the ambient temperature range of 0 to 40 °C and are applicable for Fixed, Simulator, and Table modes

			E4361A	E4362A	E4362A-J01	E4362A-J02
Output ratings (Simulator and table mode)		Maximum power	510 W	600 W	594 W	594 W
		Maximum open circuit voltage (V_{oc})	65 V	130 V	117 V	120 V
		Maximum voltage point (V_{mp})	60 V	120 V	108 V	110 V
	Line voltage: 200 V/230 V/240 V	Maximum short circuit current (I_{sc})	8.5 A	5.0 A	5.5 A	5.4 A
		Maximum circuit point (I_{mp})[1]	8.5 A	5.0 A	5.5 A	5.4 A
	Line voltage: 100 V/120 V[4]	Maximum short Circuit current (I_{sc})	4.25 A	2.5 A	2.75 A	2.7 A
		Maximum current point (I_{mp})[1]	4.25 A	2.5 A	2.75 A	2.7 A
Output ratings (Fixed mode)	**Minimum impedance (ΔV/ΔVI)**[1]		0.25 Ω	1 Ω	1 Ω	1 Ω
	Voltage		0 - 60 V	0 - 120 V	0 - 108 V	0 - 110 V
	Line voltage: 200 V/230 V/240 V	Current	0 - 8.5 A	0 - 5.0 A	0 - 5.5 A	0 - 5.4 A
	Line voltage: 100 V/120 V[4]	Current	0 - 4.25 A	0 - 2.5 A	0 - 2.75 A	0 - 2.7 A
Current derating factor (from 40 to 55 °C)			0.11 A/°C	0.069 A/°C	0.069 A/°C	0.068 A/°C
Output voltage ripple & noise (from 20 Hz to 20 MHz with a resistive load, outputs ungrounded, or either output grounded)		Simulator/table mode	20 mV_{rms}	24 mV_{rms}	24 mV_{rms}	24 mV_{rms}
			125 mV_{p-p}	195 mV_{p-p}	195 mV_{p-p}	195 mV_{p-p}
		Fixed mode (constant voltage)	24 mV_{rms}	30 mV_{rms}	30 mV_{rms}	30 mV_{rms}
			150 mV_{p-p}	150 mV_{p-p}	150 mV_{p-p}	150 mV_{p-p}
Programming accuracy[2,3] (@ 23 ±5 °C)		Fixed mode voltage	0.075% + 25 mV	0.075% + 50 mV	0.075% + 50 mV	0.075% + 50 mV
		Fixed mode current	0.2% + 20 mA	0.2% + 10 mA	0.2% + 11 mA	0.2% + 11 mA
Readback accuracy[3] (from front panel or over GPIB with respect to actual output @ 23 ±5 °C)		Voltage	0.08% + 25 mV	0.08% + 50 mV	0.08% + 50 mV	0.08% + 50 mV
		+Current	0.20% + 20 mA	0.20% + 10 mA	0.20% + 11 mA	0.20% + 11 mA
		–Current	0.35% + 48 mA	0.35% + 24 mA	0.35% + 26 mA	0.35% + 26 mA
Load regulation – fixed mode (change in output voltage or current for any load change within ratings)		Constant voltage	2 mV	2 mV	2 mV	2 mV
		Constant current	1 mA	1 mA	1 mA	1 mA
Line regulation – fixed mode (change in output voltage or current for any line voltage change within ratings)		Constant voltage	2 mV	2 mV	2 mV	2 mV
		Constant current	1 mA	1 mA	1 mA	1 mA

1. There is no maximum impedance restriction. The programmed value for Imp can be less than or equal to I_{sc}.
2. In Simulator mode, the output current is related to the readback output voltage by an internal algorithm. In Table mode, the output current is related to the readback output voltage by interpolation between points that are entered by the user.
3. The unit may go out of specification when subjected to RF fields of 3 volts/meter in the frequency range of 26 MHz to 1 GHz.
4. There is no current derating when only one output module is installed in the mainframe.